J. metamorphic Geol., 2009, **27,** 249–279 doi:10.1111/j.1525-1314.2009.00816.x

Interplay between equilibrium and kinetics in prograde metamorphism of pelites: an example from the Nelson aureole, British Columbia

D. R. M. PATTISON[1] AND D. K. TINKHAM[2]
[1]*Department of Geoscience, University of Calgary, Calgary, Alberta, T2N 1N4, Canada (pattison@ucalgary.ca)*
[2]*Department of Earth Sciences, Laurentian University, Sudbury, Ontario, Canada*

ABSTRACT The distribution of metapelitic mineral assemblages in the Nelson aureole, British Columbia, generally conforms to what is predicted from phase equilibria. However, in detail, the sequence and spacing of isograds, mineral textures and mineral compositions and mineral chemical zoning do not. Two of the main disequilibrium features in the aureole are: (i) delay in the onset and progress of several reactions, i.e. overstepping in temperature; and (ii) unreactivity of staurolite and especially garnet porphyroblasts when they are reactants in prograde reactions. The thermal overstepping is ascribed to difficulty of nucleation of the product porphyroblasts and sluggishness of dissolution of porphyroblasts when they are reactants. The extent to which these kinetic barriers delay the onset of reaction is related to the reaction affinity of each reaction, defined herein as the Gibbs free-energy difference between the thermodynamically stable, but not-yet-crystallized, products and the metastable reactants. For oversteps in temperature (ΔT), reaction affinity is, in turn, related to the difference in entropy (ΔS) between these two states through the relation $A = \Delta T * \Delta S$. Mineral reactions which release large quantities of H_2O, such as chlorite-consuming reactions, have a higher entropy change per unit of temperature overstep, and therefore a higher reaction affinity, than those which release little or no H_2O, such as the chlorite-free staurolite-consuming reaction. Thermal overstepping is consequently expected to be less for the former than for the latter, as was estimated in the aureole where 0 to 30 °C overstepping was required for garnet, staurolite and andalusite growth from a muscovite + chlorite-bearing precursor rock and ~70 °C overstepping was required for the growth of Al_2SiO_5 from a staurolite-bearing, chlorite-free precursor. In all cases, reaction progress was strongly influenced by the presence or absence of fluid, with presence of fluid lowering kinetic barriers to nucleation and growth and therefore the degree of thermal overstepping. Textural features of rocks from the nearly coincident garnet, staurolite and andalusite isograds are suggestive of a fluid-catalysed 'cascade effect' in which reaction took place in a narrow temperature interval; several competing muscovite + chlorite-consuming reactions, some metastable, appear to have occurred in parallel. Metamorphic reaction, fluid release and possibly fluid presence in general in the aureole were episodic rather than continuous, and in several cases well removed from equilibrium conditions. The extent to which these findings apply to regional metamorphism depends on several factors, a major one being enhanced deformation, which is expected to lower kinetic barriers to nucleation and growth.

Key words: equilibrium; kinetics; metamorphic reactions; overstepping; reaction affinity.

INTRODUCTION

This study addresses the interplay between the approach to equilibrium and reaction kinetics during prograde metamorphism of pelites. It expands on some of the ideas of Waters & Lovegrove (2002), who argued for reaction overstepping on the order of 30–40 °C for the production of staurolite and andalusite from a precursor assemblage of muscovite, chloritoid and chlorite in pelites from the Bushveld aureole. They ascribed the overstepping to a combination of sluggish porphyroblast nucleation and sluggish dissolution of precursor chloritoid, laying special emphasis on the former. Their study of the Bushveld rocks showed that: (i) thermally activated devolatilization reactions can be significantly overstepped even when the observed mineral assemblages conform closely to predictions from equilibrium thermodynamics, and (ii) the actual reactions involved in the formation of a stable equilibrium assemblage can be considerably different from those predicted by equilibrium modelling.

This study expands on some of these ideas using the Nelson aureole, British Columbia (Pattison & Vogl, 2005) as an example. We focus on two main issues: (i) contrasts in the degree of overstepping in temperature

of pelitic reactions as a function of reaction affinity and fluid presence; and (ii) the relative unreactivity of porphyroblasts, in particular garnet and staurolite, when they are reactants in prograde reactions. 'Reaction affinity' as used in this paper refers to the Gibbs free energy potential that builds up when a reaction boundary is overstepped in pressure or temperature. It represents the Gibbs free energy difference between the thermodynamically stable, but not yet crystallized, products and the metastable reactants. This energy is used to overcome kinetic barriers to nucleation and growth of the product assemblage. For oversteps in temperature (ΔT), reaction affinity is, in turn, related to the entropy difference (ΔS) between these two states, through the relation $A = \Delta T * \Delta S$, where $\Delta T = T - T_{eq}$. Reaction affinity, per unit of temperature overstep, is therefore higher for high-ΔS reactions, such as devolatilization reactions, than for low-ΔS reactions, such as solid–solid reactions. For the same energetic threshold for reaction, high-ΔS reactions are predicted to be overstepped less than low-ΔS reactions.

In this study, we contrast the formation of staurolite and andalusite from a muscovite + chlorite-bearing precursor assemblage (high ΔS, non-porphyroblastic reactants, low predicted thermal overstepping) with the formation of andalusite from a chlorite-free, staurolite-bearing precursor assemblage (low ΔS, porphyroblastic reactants, higher predicted overstepping). The significant overstepping of initial garnet formation from a muscovite + chlorite-bearing precursor assemblage is also discussed. It is argued that, in all cases, fluid presence, whether introduced or generated internally, had a major effect on the degree of thermal overstepping. At the end of the paper, some of the broader implications of our findings are discussed.

THE NELSON BATHOLITH AND AUREOLE

The Nelson Batholith is one of the largest of a suite of middle Jurassic plutons in south-eastern British Columbia (e.g. Archibald *et al.*, 1983). The batholith is emplaced in Triassic–Jurassic graphitic argillaceous rocks that were regionally deformed and metamorphosed to biotite zone conditions in the Jurassic, prior to intrusion of the batholith.

The composite batholith ranges from tonalite to granite and comprises a northern mass, including the Mt. Carlyle Stock, of about 30×50 km^2 (referred to as the 'main body') and a 25 km long southern 'tail' (Little, 1960; Vogl & Simony, 1992) (Fig. 1a). U-Pb dating indicates that the different phases of the batholith were intruded in the Jurassic between *c.* 173 and 159 Ma (Parrish, 1992; Sevigny & Parrish, 1993; Ghosh, 1995). Geophysical and petrological data indicate that the batholith is a tabular, flat-bottomed body, 2 to 7 km below the present-day sea level (Cook *et al.*, 1988). The batholith and aureole are tilted $\sim$10° to the west, with the tilting ascribed to a combination of Jurassic–Cretaceous contractional deformation and Eocene extension (Pattison & Vogl, 2005).

A 0.7–1.8 km wide contact aureole surrounds the batholith. Different prograde metapelitic mineral assemblage sequences are developed in the argillaceous host rocks around the aureole in a regular pattern, reflecting different pressures of contact metamorphism arising from the post-metamorphic tilting (Pattison & Vogl, 2005). Higher-pressure staurolite ± andalusite-bearing mineral assemblage sequences are restricted to the aureole surrounding the eastern half of the batholith, whereas lower-pressure cordierite ± andalusite-bearing mineral assemblage sequences are restricted to the aureole surrounding the western half of the batholith and its northern and southern tips (Fig. 1a). Despite the differences in mineral assemblage sequences in the aureole, the total pressure difference between them is only about 1.0 kbar (Fig. 1a; Pattison & Vogl, 2005). U-Pb dating of monazite that was produced during contact metamorphism is the same age, within error, as the intrusion (Tomkins & Pattison, 2007).

PROGRADE METAMORPHISM IN THE STUDY AREA

Figure 1b shows the part of the aureole examined in this study, corresponding to Area D of Pattison & Vogl (2005), but showing more isograds and incorporating more recent sampling. A general description of the metamorphic zones, accompanied by photomicrographs, is provided in Pattison & Vogl (2005).

The sequence of mineral-in isograds in the study area is garnet, staurolite ± andalusite, sillimanite, K-feldspar, with the garnet, staurolite and andalusite isograds coincident in some places at the level of the spatial resolution allowed by the sampling (Fig. 1b). Migmatization, interpreted to be due to partial melting, is associated with the development of K-feldspar (Pattison & Vogl, 2005). The above prograde sequence is a classic facies series 2b (staurolite–andalusite) sequence in the scheme of Pattison & Tracy (1991), and represents a pressure of formation of $\sim$3.5–4.0 kbar assuming the Pattison (1992) Al_2SiO_5 triple point or $\sim$2.5–3.0 kbar assuming the Holdaway (1971) triple point.

Below, the salient features of each zone are described, with emphasis on the textures of garnet, staurolite and andalusite and the chemical zoning in garnet. These observations are then compared with predictions from thermodynamic modelling later in the paper. Figure 2 shows garnet and staurolite textures at different grades in the aureole. Figure 3 shows textures of rocks from the andalusite and sillimanite zones. Figures 4 to 10 show garnet chemical zoning in rocks from the garnet, staurolite, andalusite, sillimanite and K-feldspar zones.

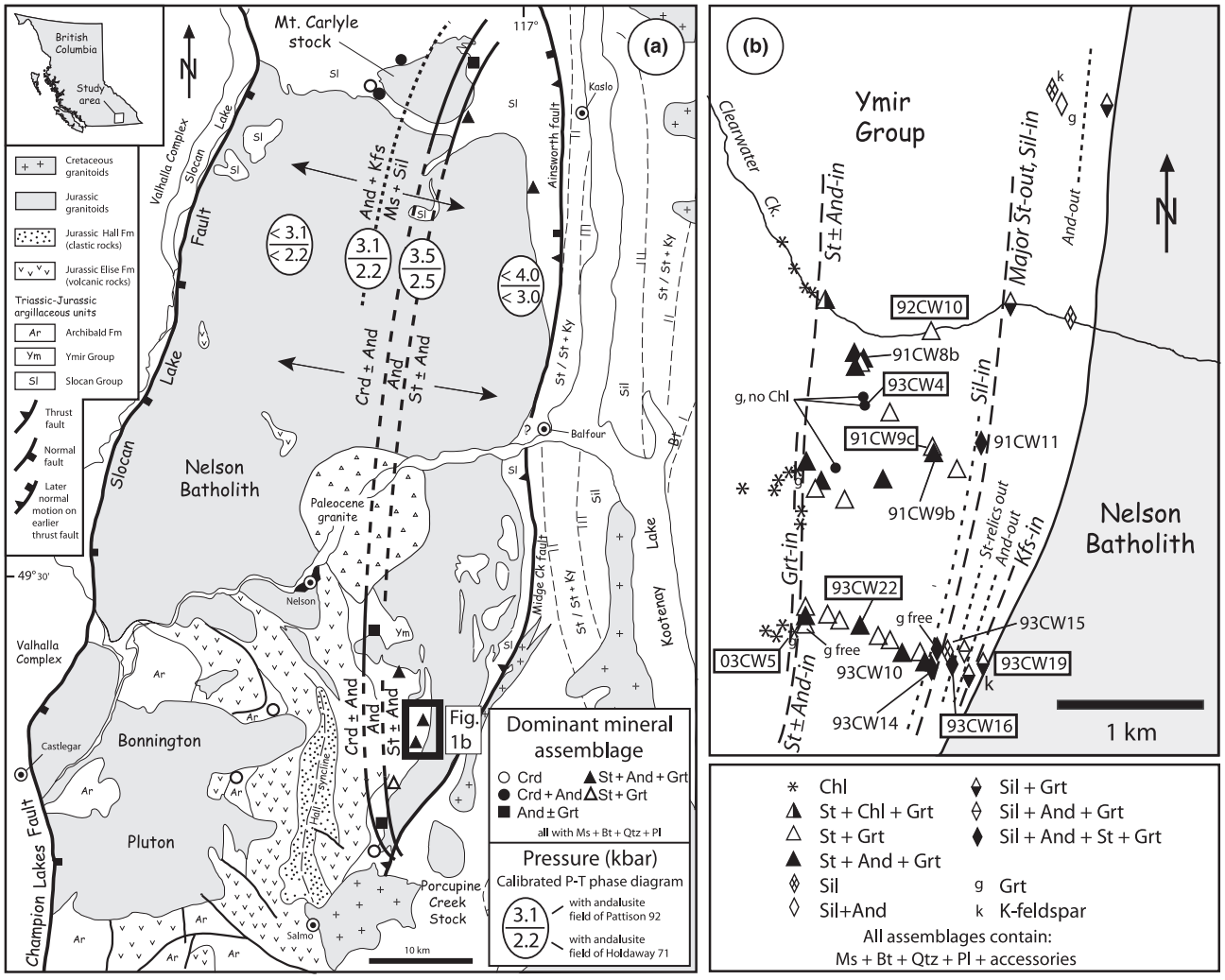

Fig. 1. (a) Regional map of the Nelson batholith and aureole, adapted from Pattison & Vogl (2005). Dashed lines separate mineral assemblage domains of different pressure (see Pattison & Vogl, 2005; for details). (b) Mineral assemblages and isograds from the study area. Sample numbers in boxes – samples analysed chemically and presented in Figs 4–10. Sample numbers without boxes – samples for which photomicrographs are presented in Figs 2 & 3.

Mineral compositions and chemical zoning

Two or three representative garnets from each rock were compositionally mapped and quantitatively analysed. These were typically the largest garnets in the thin section. Garnet was mapped for Fe, Mn, Mg, Ca and Y on the JEOL JXA-8200 electron microprobe at the University of Calgary under the following conditions: focused beam; 15 kV; 500 nA; 100 ms dwell time; 2 μm pixel size. Quantitative garnet analyses were performed using wavelength-dispersive analysis under the following conditions: focused beam; 15 kV; 50 nA; peak and background dwell times of 20 and 10 s, respectively, for Fe, Mn, Mg, Ca, Al, Si and 40 and 20 s, respectively, for Y, P and Ti. Compositions of other minerals (biotite, muscovite, staurolite and plagioclase) are provided in Pattison & Vogl (2005).

Regional metamorphic rocks outside the aureole

The host rocks outside the aureole in the study area are regionally deformed and metamorphosed graphitic, locally sulphide-rich, argillites of the Triassic to Early Jurassic Ymir Group (Cairnes, 1934; Little, 1960; Archibald *et al.*, 1983; Pattison & Vogl, 2005). The argillites are variably interbedded with quartzite, siltstone and dark, graphitic marble. The regional metamorphic grade is the biotite zone. Most of the argillites outside the aureole contain biotite, but none contains garnet. The rocks also contain chlorite, quartz, muscovite, plagioclase and graphite, in addition to some or all of ilmenite, tourmaline, zircon, monazite, pyrrhotite, xenotime and allanite. Whole-rock chemical analysis of the argillites shows a narrow compositional range (Pattison & Vogl, 2005).

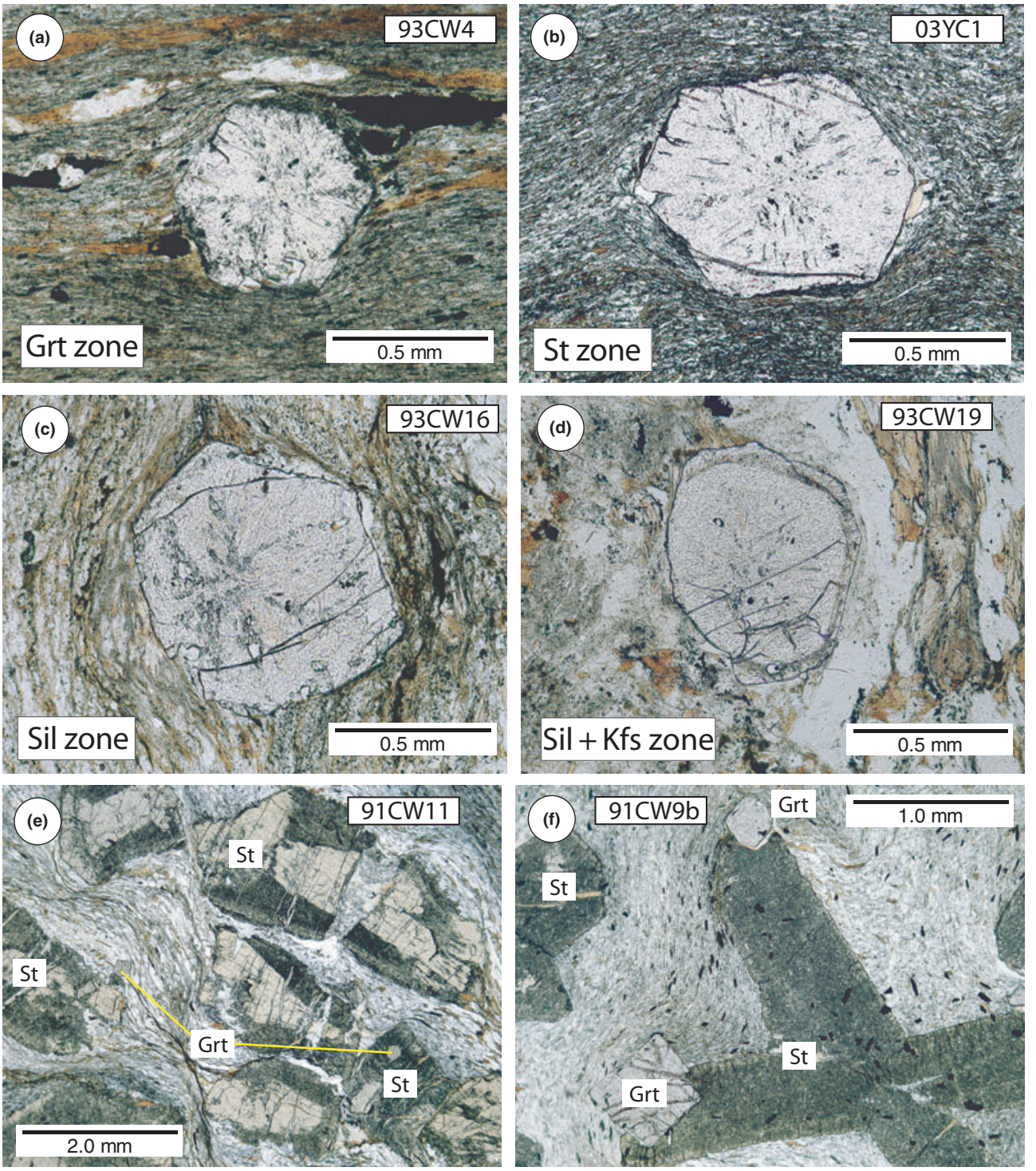

Fig. 2. Textures of garnet (a–d) and of staurolite (e–f). Sample localities shown in Fig. 1b. See text for discussion of images.

Garnet zone

The garnet zone in Fig. 1b is narrow (< 50 m) to non-existent, within the resolution of the sampling, even though garnet is widespread in assemblages at higher grade and from textural features formed before the other porphyroblasts. The idealized reaction that forms garnet, in the model pelitic chemical system KFMASH (K_2O-FeO-MgO-Al_2O_3 SiO_2-H_2O), is:

$$Ms + Chl + Qtz = Grt + Bt + H_2O. \quad (1)$$

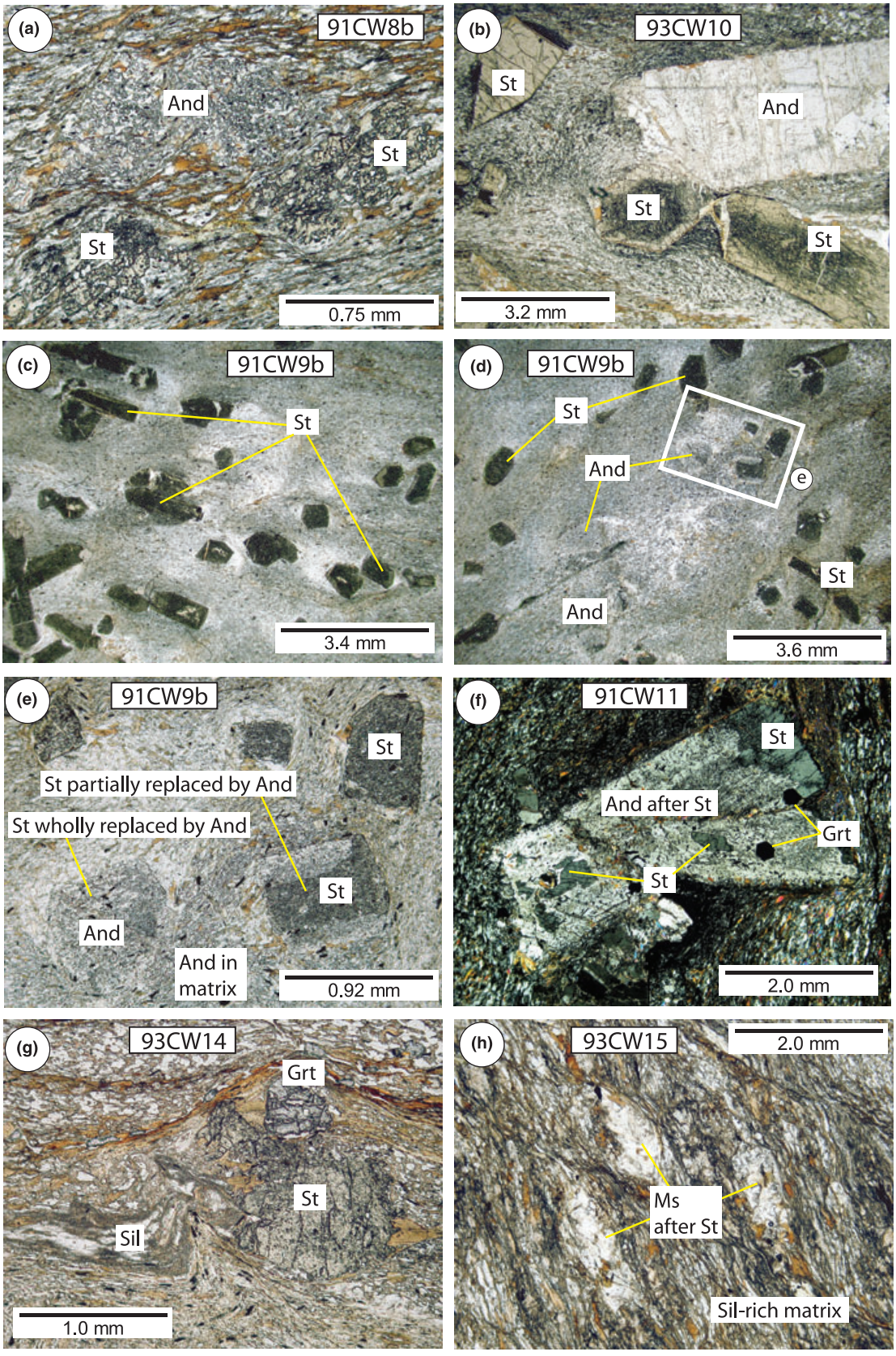

Fig. 3. Textures of andalusite- and sillimanite-bearing rocks. Sample localities shown in Fig. 1b. See text for discussion of images.

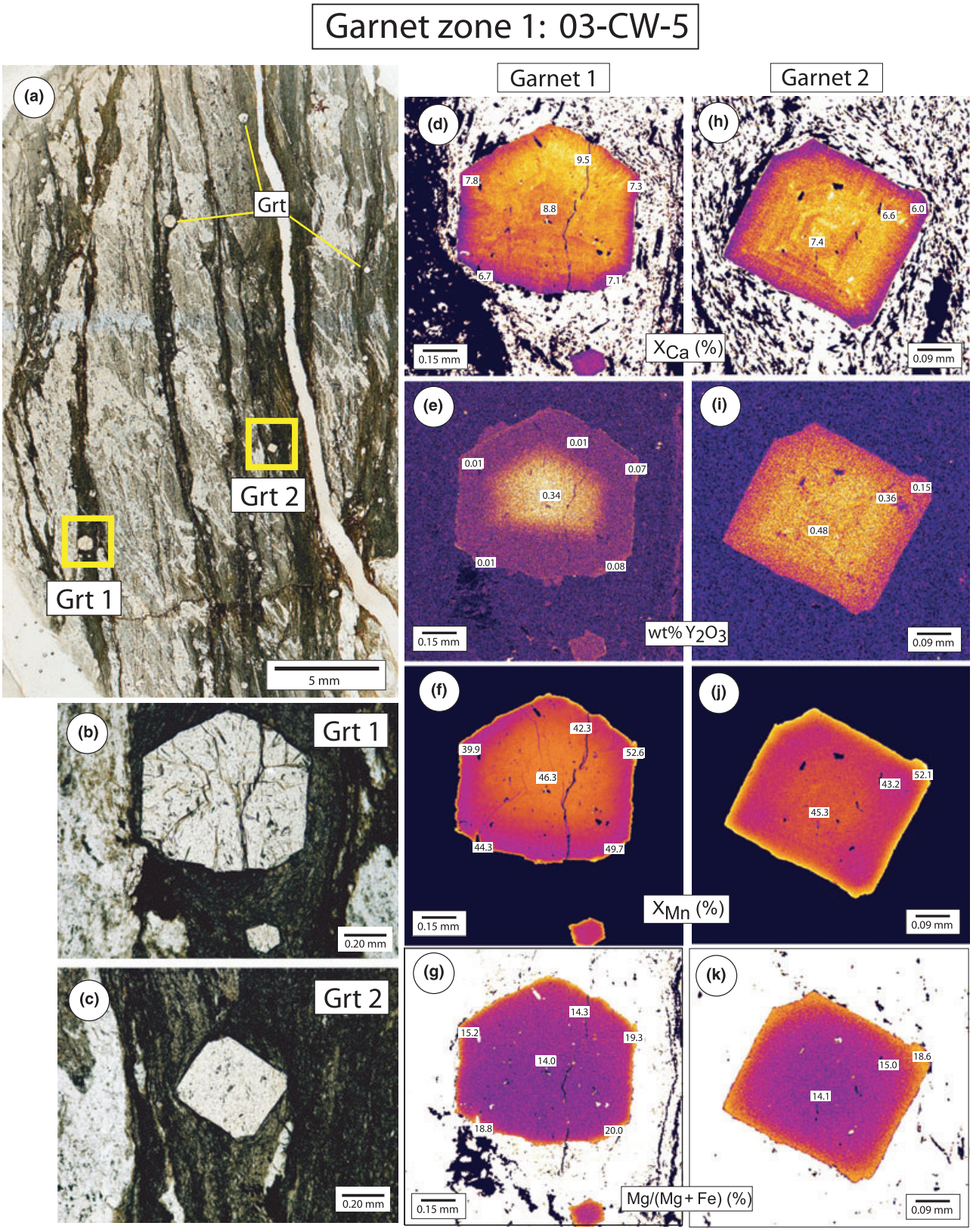

Fig. 4. Photomicrographs, compositional maps and compositional analyses of garnet from the garnet zone, sample 03CW5 (see Fig. 1b for location of sample).

Figures 2, 4 and 5 show photomicrographs and garnet chemical zoning maps of two rocks from the garnet zone (03CW5 & 93CW4; Fig. 1b). Although 93CW4 is physically within the staurolite zone, it contains no staurolite or primary chlorite, suggesting that the chlorite needed for staurolite formation was consumed beforehand during the formation of the garnet in reaction (1).

Garnet is restricted to phyllosilicate-rich layers in 03CW5 whereas it is more evenly distributed through the rock in 93CW4. The garnet in both samples shows macroscopically rational crystal face development, but that in 03CW5 is relatively inclusion-free whereas that in 93CW4 has inclusion-filled rims. In thin section a conspicuous internal textural feature in garnet from both samples, especially in 93CW4, is a radial, hexagonal growth pattern outlined by fine inclusions of quartz, graphite and accessory phases (Figs 2 & 5b,c). Such a pattern has been observed in a number of other localities (e.g. Andersen, 1984; Burton, 1986; Rice & Mitchell, 1991; Jamtveit & Andersen, 1992; Yardley *et al.*, 1996; Wilbur & Ague, 2006) and has been ascribed to porphyroblast growth under hydrostatic conditions in graphitic rocks, possibly accompanied by relatively rapid growth. This distinctive pattern is discernible in garnet at all grades (Fig. 2a–d), suggesting that the mechanism of garnet growth even in high-grade rocks was similar to that now seen in rocks from the garnet zone.

The radial inclusion texture is accompanied by a subtle radial pattern in Ca concentration in which thin, outwardly emanating, flame-like zones of slightly higher and lower Ca concentration extend across the more dominant concentric zones of differing Ca concentration (Figs 4 & 5). The origin of these radial textures is unknown but, by analogy with the radial inclusion patterns noted above and with sector chemical zoning observed in igneous minerals, it may also be an indicator of relatively rapid growth of garnet.

In both samples, the dominant feature of Ca concentration is an irregular, broadly oscillatory zoning from generally higher values in the centres to lower values at the rims (Figs 4 & 5). Explanations for this type of oscillatory zoning are several (e.g. Chernoff & Carlson, 1997; Meth & Carlson, 2005), but the zoning suggests processes more complex than those predicted from simple thermodynamic modelling, as discussed below. Yttrium zoning varies both between and within the samples, suggestive of local (sub-millimetre) variations in Y concentration and lack of thin-section scale equilibration.

In the garnet from 93CW4, Mn shows a typical bell-shaped pattern of decreasing Mn concentration away from the core. Mg/(Mg + Fe) shows a slight increase from core to rim followed by a drop at the outer rim (Fig. 5g). The situation is similar in the garnet from 03CW5 except that within a few tens of microns of the rims there is a sharp increase in both Mn concentration and Mg/(Mg + Fe).

The lack of other porphyroblasts in the rocks and the euhedral texture of the garnet indicate that these patterns are due to growth rather than resorption. A possible explanation for prograde Mn-enrichment at the rims of the garnet in 03CW5 is consumption of ilmenite during garnet growth. Ilmenite with Mn/(Mn + Fe) = 0.18 occurs as inclusions in garnet cores but is absent from the matrix, whereas rutile does not occur as garnet inclusions but is present in the matrix. In this pyrrhotite-bearing, S-rich rock (0.49 wt% S), the reaction of ilmenite to rutile may have been accompanied by the reaction of pyrite to pyrrhotite by the coupled Fe-, S- and Ti-conserving reaction, Ilm + Py = Rut + 2 Po (Connolly & Cesare, 1993). The Mg-enrichment in the garnet rims could also be explained by this reaction, in which some of the Fe sequestered by pyrrhotite may have come from co-reacting silicate minerals like chlorite, resulting in concomitant growth of relatively magnesian garnet.

Staurolite zone

A separate staurolite zone, defined by rocks containing staurolite but lacking andalusite, cannot be identified because the lowest grade occurrences of andalusite and staurolite are in the same outcrops (Fig. 1b). However, there is a substantial, 800–1200 m wide domain upgrade of the staurolite ± andalusite isograd in which staurolite-bearing, andalusite-free mineral assemblages are common. Textural evidence indicates that staurolite growth preceded andalusite growth. Consequently, we refer to the abundant staurolite-bearing, andalusite-free rocks as belonging to the staurolite zone for simplicity.

Figures 6 and 7 show photomicrographs and maps of garnet chemical zoning of two representative andalusite-free rocks from the staurolite zone (92CW10 & 91CW9c; Fig. 1b). The staurolite in 92CW10 is unaltered whereas many grains of staurolite in 91CW9c are partially replaced by muscovite intergrown with lesser amounts of biotite (Fig. 7a).

Garnet appears generally euhedral–subhedral in 92CW10, although corners and edges of crystals in the matrix show evidence of rounding (Fig. 6a,b). In contrast, garnet enclosed within staurolite shows sharp corners (Fig. 6c). In 91CW9c, all garnet is sharply euhedral (Fig. 7).

Ca zoning in garnet from 92CW10 is dominated by concentric oscillatory-type zoning, with a ~0.05 mm-wide annulus of slightly higher Ca concentration at the margins. Superimposed on this pattern are the same patchy, flame-like features seen in the garnet zone. Yttrium mimics the concentric Ca patterns, showing high core values and low marginal values, with a narrow annulus of elevated concentration within the low-Y margin. The origin of this Y pattern was ascribed to successive breakdown of xenotime (high-Y core) and allanite (Y annulus) during garnet growth (Tomkins & Pattison, 2007). In 91CW9c, Ca zoning

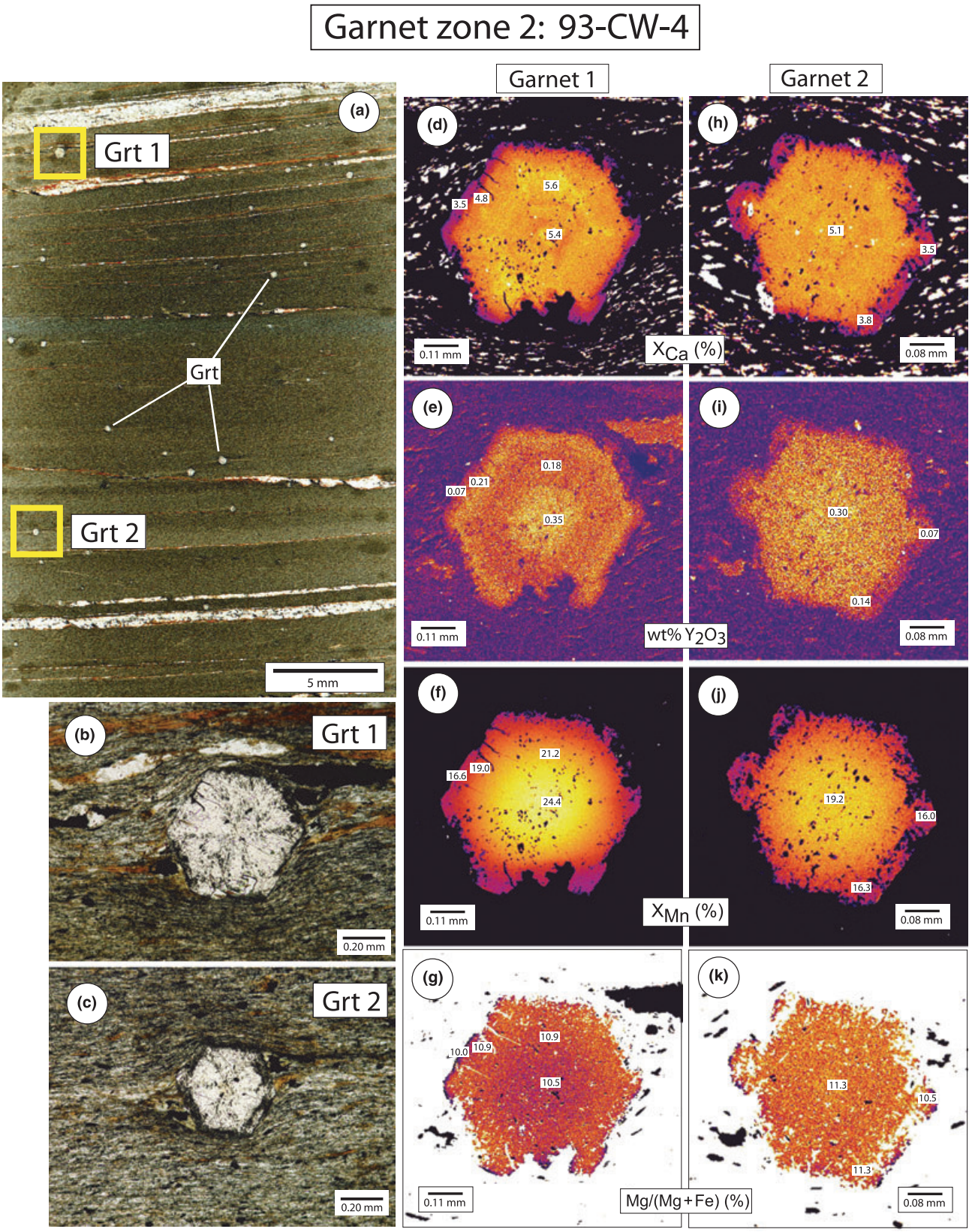

Fig. 5. Photomicrographs, compositional maps and compositional analyses of garnet from the garnet zone, sample 93CW4 (see Fig. 1b for location of sample).

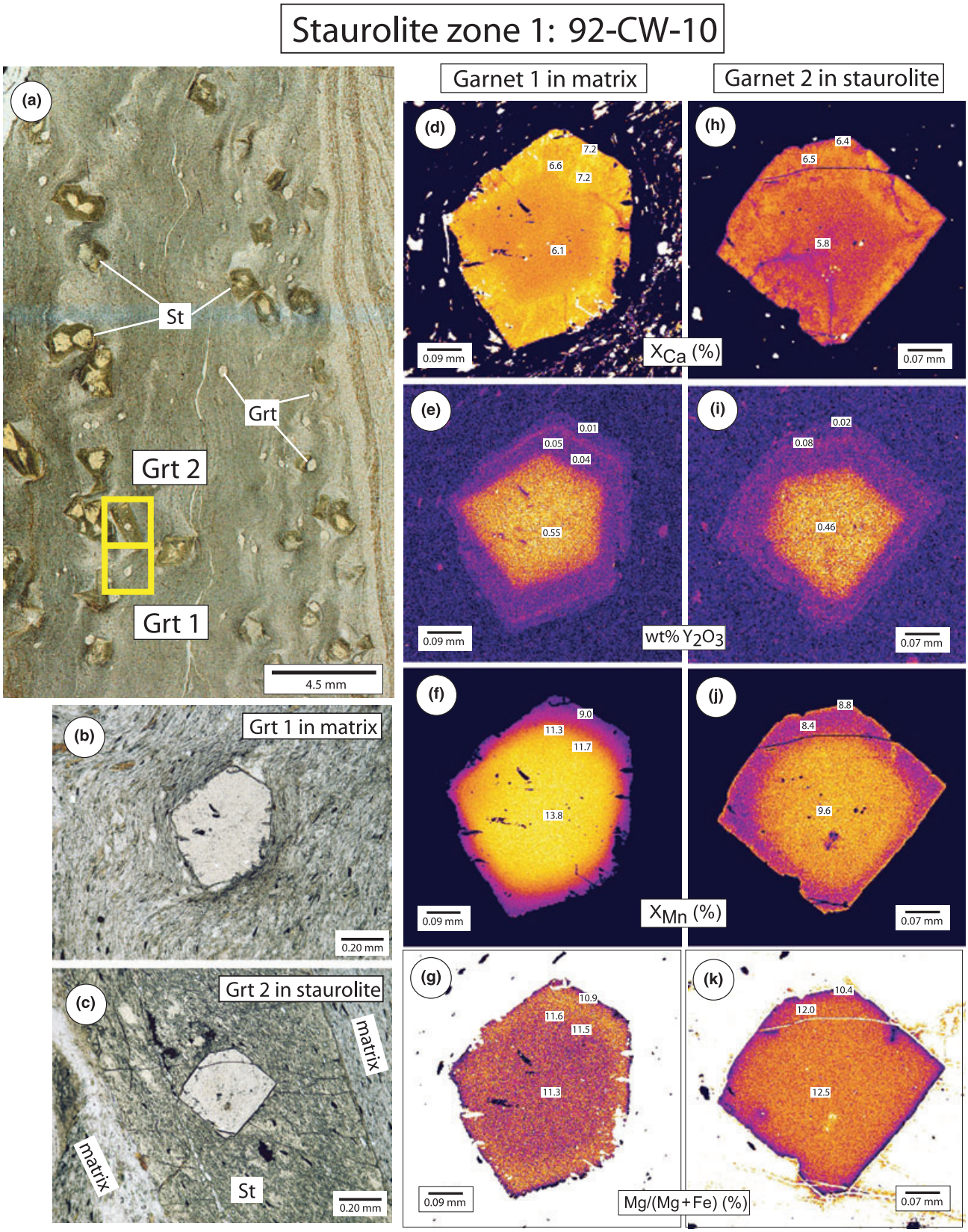

Fig. 6. Photomicrographs, compositional maps and compositional analyses of garnet from the staurolite zone, sample 92CW10 (see Fig. 1b for location of sample).

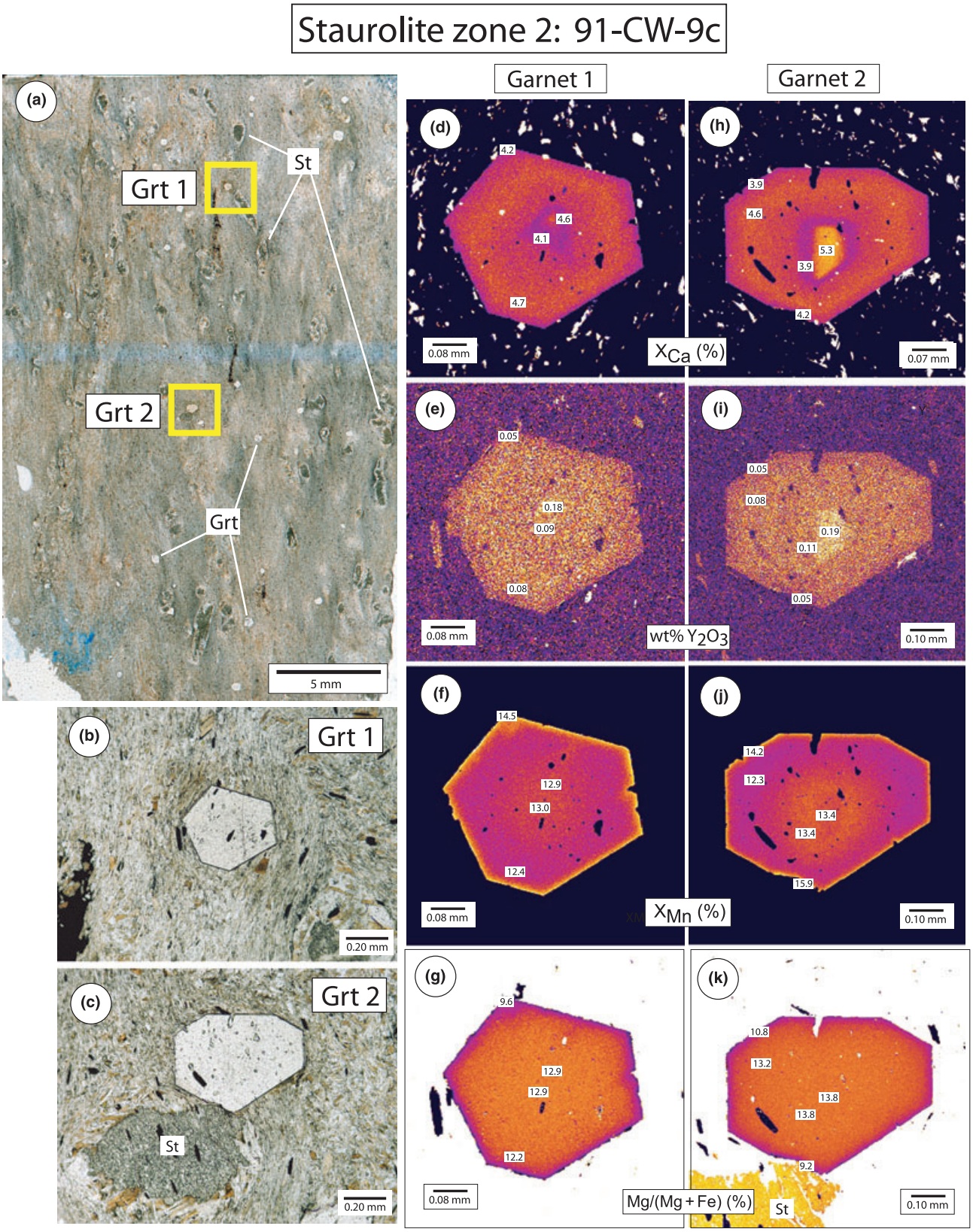

Fig. 7. Photomicrographs, compositional maps and compositional analyses of garnet from the staurolite zone, sample 91CW9c (see Fig. 1b for location of sample).

also shows concentric variations but none of the radial features seen in 92CW10, and Y mimics Ca. The idealized reaction forming staurolite is:

$$Ms + Grt + Chl + Qtz = St + Bt + H_2O. \quad (2)$$

However, textural evidence for the participation of garnet in this reaction is minimal. In 92CW10 (Fig. 6), even the garnet showing rounded corners and edges, which might be taken as evidence for dissolution, shows internal growth zones defined by Ca and Y that have similar rounded corners and edges, suggesting that the crystals may never have developed sharp corners and edges. The best evidence for dissolution comes from the truncation of Y and Ca zoning on the left side of the crystal in Fig. 6d,e. Despite the evidence for dissolution, there is no evidence for Mn-enrichment at this edge. In 91CW9c, the textures and chemical zoning suggest no garnet dissolution whatsoever. We therefore conclude that the reaction that best accounts for staurolite development is:

$$Ms + Chl + Qtz = St + Bt + H_2O. \quad (3)$$

Andalusite zone

The location of the andalusite isograd is indistinguishable from that of the staurolite isograd within the resolution of the sampling. The andalusite zone extends 900 m up to the sillimanite zone. Andalusite occurs in three main textural varieties (Fig. 3).

1 In samples from the lower grade part of the andalusite zone (e.g. 91CW8b in Fig. 1b), it grows as anhedral poikiloblasts scattered through the rock, accompanied by staurolite porphyroblasts of similar anhedral poikiloblastic texture and by small euhedral garnet porphyroblasts (Fig. 3a).

2 In the middle and upper andalusite zone, andalusite commonly occurs as discrete, chiastolitic porphyroblasts, sometimes with inclusions of euhedral staurolite (Figs 3b & 8a of this study, and fig. 6b of Pattison & Vogl, 2005). Staurolite porphyroblasts in the matrix of the rocks are commonly euhedral as well.

3 In the middle and upper andalusite zone, andalusite occurs as partial or complete pseudomorphs of staurolite porphyroblasts (Figs 3d–f).

More than one variety of andalusite may occur in the same rock (e.g. Fig. 3e of this study and fig. 6b of Pattison & Vogl, 2005).

Andalusite-free St + Bt + Grt assemblages are common within the andalusite zone and may occur in the same outcrop and even in the same thin section as andalusite-bearing assemblages. An example is shown in Fig. 3c–e. In one part of the thin section, staurolite shows no evidence for reaction whatsoever (Fig. 3c), whereas millimetres away, staurolite porphyroblasts may be completely converted to pseudomorphs of andalusite (Fig. 3d). Intermediate stages, consisting of partial pseudomorphing of staurolite by andalusite, occur between the two extremes (Fig. 3e). Electron microprobe analysis shows that there is no compositional difference between the reacting staurolite and the unreacted staurolite, suggesting kinetic control.

Figure 8 shows maps of garnet chemical zoning from a representative andalusite-bearing rock exhibiting andalusite textural varieties 2 and 3 (93CW22; Fig. 1b). Two garnets were mapped: one in the matrix and a second included in andalusite. Examining the matrix garnet (Fig. 8d–g), the Ca zoning of the inner part is similar to that of the staurolite zone sample 92CW10. In contrast, however, is a distinct outermost rim of lower-Ca garnet. Boundaries between the three Ca domains are spatially matched by changes in Y content (Fig. 8e), with a narrow Y annulus developed at the interface between the outer low-Ca rim and the inner higher-Ca domains.

The garnet included in andalusite (Fig. 8h–k) shows similar Ca and Y zoning except that the outer domain of low Ca is restricted to the side of the garnet facing away from the centre of the enclosing andalusite. This asymmetry most likely arises from the fact that the side of the garnet closest to the middle of the enclosing andalusite crystal side was armoured fairly early on during andalusite growth, in contrast to the side facing into the matrix which was open to new, low-Ca, growth on its outer margin.

The idealized reaction forming andalusite is:

$$Ms + St + Qtz = And + Grt + Bt + H_2O. \quad (4)$$

Evidence for this reaction is seen locally in replacement of staurolite by andalusite, and the development of a conspicuous low-Ca rim on garnet which is absent from andalusite-free, staurolite-bearing rocks. However, andalusite varieties 1 and 2 seem to have grown without any significant dissolution of staurolite, which may reflect growth from matrix muscovite and chlorite in a reaction such as:

$$Ms + Chl + Qtz = And + Bt + H_2O. \quad (5)$$

Sillimanite zone

The sillimanite isograd occurs 400 m from the intrusive contact and is marked by small amounts ($<<1$ modal%) of fibrolitic and fine-grained sillimanite (see Pattison, 1992; p. 426–427, for a discussion of the distinction between the two). The sillimanite occurs in the matrix and on the margins of andalusite and staurolite porphyroblasts (Fig. 3g).

Three hundred metres from the contact, the rock texture changes abruptly, taking on a more schistose, less porphyroblastic appearance than at lower grade, and sillimanite is abundantly developed. Staurolite and andalusite porphyroblasts are replaced by coarse muscovite commonly containing sillimanite needles (Figs 3h & 9 of this study and fig. 6e of Pattison & Vogl, 2005). The coincidence of textural change, staurolite consumption and abundant sillimanite development is shown in Fig. 1b as the 'major staurolite-out, sillimanite-in' isograd. Staurolite relics

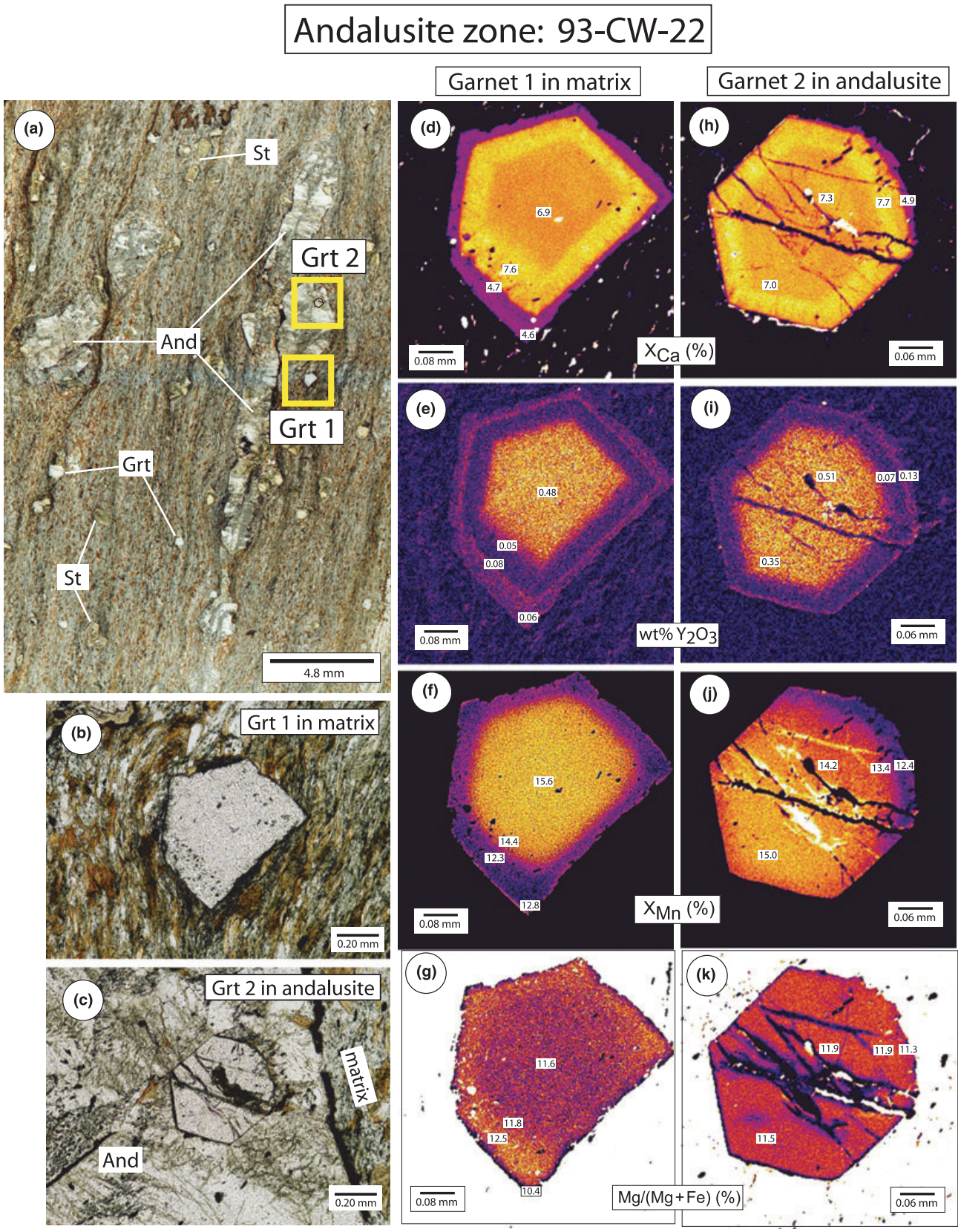

Fig. 8. Photomicrographs, compositional maps and compositional analyses of garnet from the andalusite zone, sample 93CW22 (see Fig. 1b for location of sample).

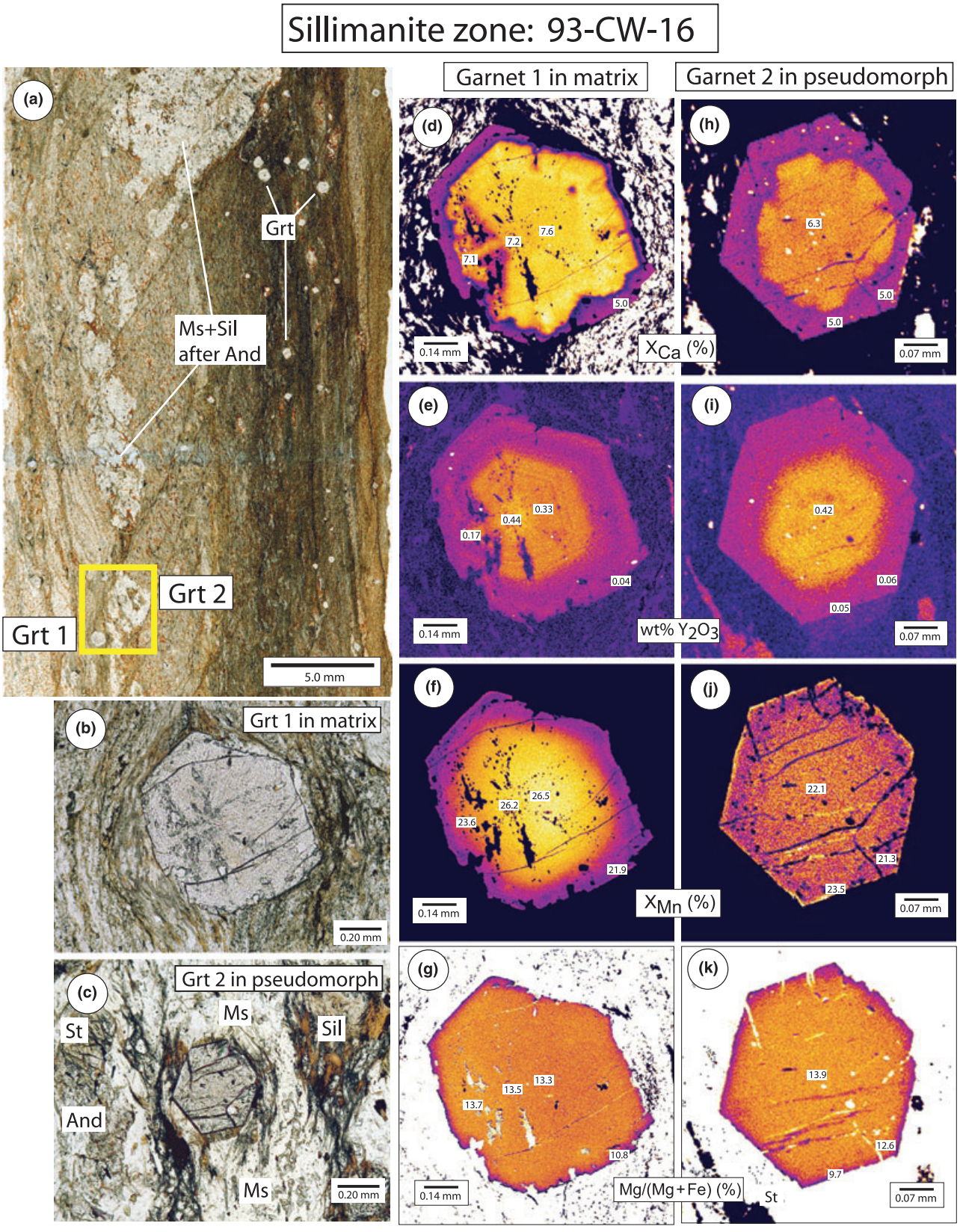

Fig. 9. Photomicrographs, compositional maps and compositional analyses of garnet from the sillimanite zone, sample 93CW16 (see Fig. 1b for location of sample).

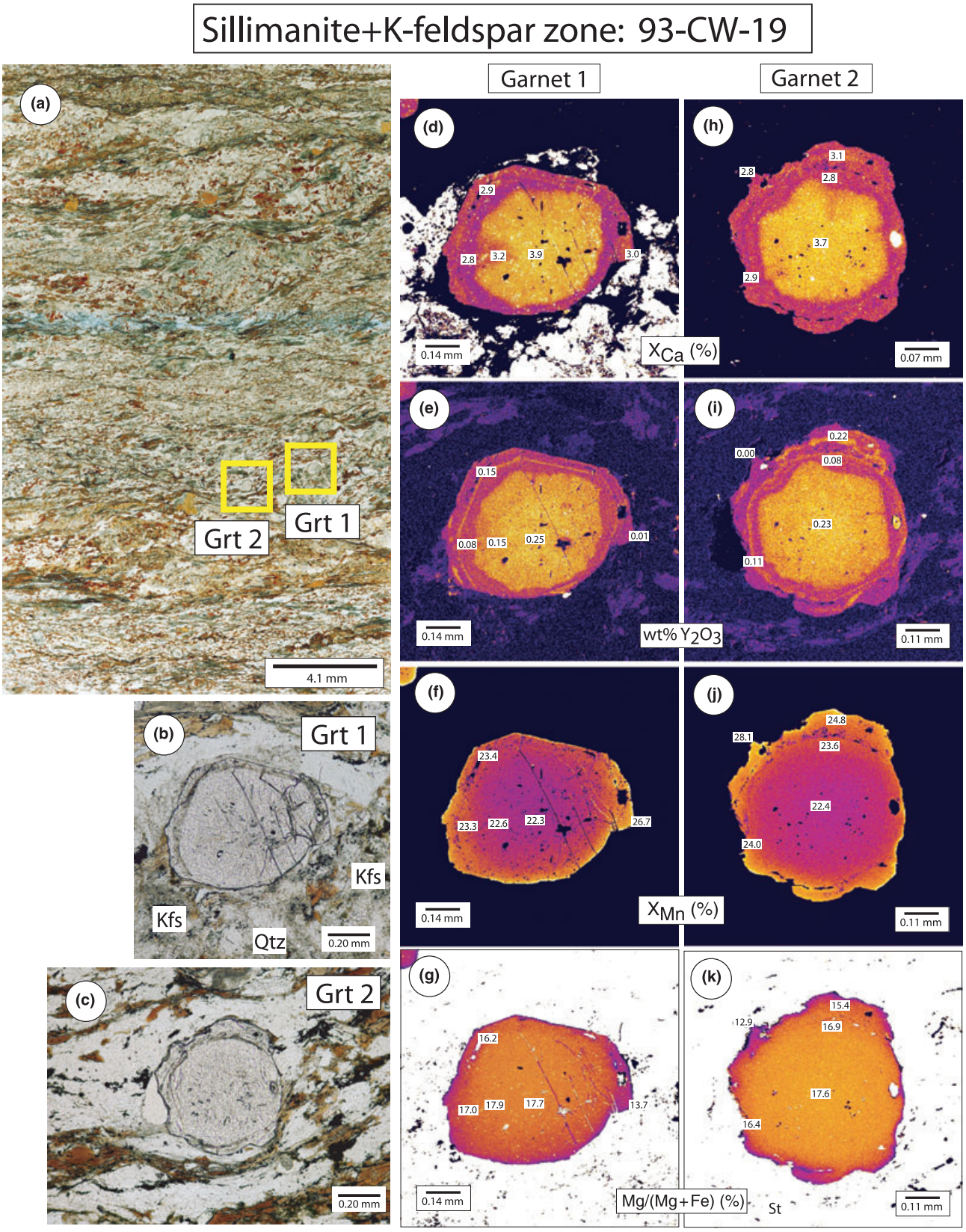

Fig. 10. Photomicrographs, compositional maps and compositional analyses of garnet from the K-feldspar zone, sample 93CW19 (see Fig. 1b for location of sample).

persist a little upgrade in some rocks (Fig. 1b). The last observed occurrence of andalusite is ~150 m from the contact, defining a zone of co-existence of And + Sil of about 250 m width.

Garnet in some rocks from the sillimanite zone shows inner portions with radial inclusion patterns similar to those seen in garnet from the garnet and staurolite zones (Fig. 2c). The rims commonly contain needles of fine-grained sillimanite (Fig. 9b,c), indicating garnet growth during or after sillimanite growth.

Figure 9 shows maps of garnet chemical zoning from a representative sillimanite-bearing rock (93CW16; Fig. 1b). Two garnets were mapped: one in the matrix and a second included in a muscovite pseudomorph (most likely after staurolite). Examining the matrix garnet (Fig. 9d–g), Ca zoning is similar to that in andalusite zone sample 93CW22, including an outermost rim of low-Ca garnet within which the sillimanite is included. Whereas in andalusite zone sample 93CW22 the interface between the high-Ca domain and the low-Ca outer rim is sharp and euhedral, in sillimanite-bearing sample 93CW16 the interface is irregular and embayed in places, suggestive of localized dissolution prior to growth of the outer rim.

Yttrium content matches the inner Ca zones (Fig. 9d,e), with an abrupt drop-off in Y matching the change from moderate Ca values in the inner core to higher values in the outer core. However, there is little change in Y concentration across the anhedral interface between the low-Ca rim and the inner higher-Ca domain where dissolution is inferred. The garnet included in the muscovite pseudomorph (Fig. 9h–k) shows broadly similar chemical zoning.

The development of abundant sillimanite in the rock matrix and within the low-Ca garnet rims, concomitant with major consumption of staurolite, suggests the following reaction:

$$\mathrm{Ms + St + Qtz = Sil + Grt + Bt + H_2O}. \quad (6)$$

The reaction responsible for the initial, modally minor development of sillimanite in rocks downgrade of the main development of sillimanite is uncertain, but may have involved reaction of matrix minerals. Andalusite shows no evidence of instability until the major staurolite-out, sillimanite-in isograd is crossed, at which point it is variably replaced by muscovite and sillimanite. Although there is little direct evidence for progress of the polymorphic inversion reaction,

$$\mathrm{And = Sil}, \quad (7)$$

this reaction may have been involved in the wholesale textural and mineralogical changes occurring at the major staurolite-out, sillimanite-in isograd.

K-feldspar zone

Within 100 m of the contact, K-feldspar occurs in the assemblage Ms + Qtz + Kfs + Sil + Bt ± Grt, marking the K-feldspar-in isograd. K-feldspar occurs in medium- to coarse-grained leucosomes consisting of anhedral, variably perthitic crystals intergrown with quartz and sillimanite (fig. 6g of Pattison & Vogl, 2005). These features are suggestive of partial melting by the reaction:

$$\mathrm{Ms + Qtz = Sil + Kfs + melt}. \quad (8)$$

Garnet in a rock from the K-feldspar zone shows inner portions with radial inclusion patterns similar to those in garnet at lower grade (Fig. 2d), mantled by anhedral–euhedral rims containing needles of fine-grained sillimanite (Fig. 10b,c). Figure 10 shows maps of garnet chemical zoning from this rock (93CW19; Fig. 1b). The zoning is more complex than at lower grade, with Ca and Y defining the following distinct zones with abrupt boundaries: an anhedral inner zone, containing the highest Ca and Y concentrations, corresponding to the zone of radial inclusions; a zone of lower Ca and Y, with a high-Y annulus at its outer edge; and an outer rim in which Ca concentration is slightly higher than the previous zone, but Y concentration is variable (compare Fig. 9e,i). High Mn and low Mg/(Mg + Fe) on the anhedral outer edge of the garnet are consistent with local resorption.

PHASE EQUILIBRIUM MODELLING

Figure 11 shows phase diagram sections calculated for the average composition of pelites from the Nelson aureole from Pattison & Vogl (2005), given in Table 1. In terms of the Thompson (1957) AFM projection, the bulk composition has an *A*-value of 0.1 and an Mg/(Mg + Fe) of 0.46. The average composition of eight pelites just from the study area appears to be slightly Fe-richer [average Mg/(Mg + Fe) = 0.44] and Mn-richer (0.092 wt% MnO *v* 0.082 wt% MnO in the average composition), but whether this difference is statistically significant is uncertain.

The thermodynamic data set used to calculate the phase diagrams is that of Holland & Powell (1998) updated to ds5.5 in 2003. Activity models used in all calculations are those used in Tinkham & Ghent (2005) with the following exceptions: (i) margarite was not considered as a component in white mica, and (ii) the ternary feldspar model of Holland and Powell (2003), using a molecular mixing model and asymmetric formalism, was used instead of separate plagioclase and pure orthoclase or sanidine.

Two phase diagram software packages were used to calculate the phase diagrams: THERMOCALC *v*. 3.25 (Powell, 1998) and THERIAK-DOMINO (De Capitani & Brown, 1987; De Capitani, 1994). For the same thermochemical database and activity models, THERIAK-DOMINO gives calculated phase boundaries to within 1–2 °C of the THERMOCALC results.

Choice of chemical system for modelling

Four chemical systems were used to model the phase equilibria (Fig. 11): MnNCKFMASHT (MnO-Na_2O-CaO-K_2O-FeO-MgO-Al_2O_3-SiO_2-H_2O-TiO_2, with C and P_2O_5 omitted from the whole-rock analysis, followed by projection from pyrrhotite); MnNCKFMASH (system reduced from MnNCKFMASHT by projection from ilmenite); MnKFMASH (system reduced from MnNCKFMASH by projection from albite and anorthite); KFMASH (system reduced from MnKFMASH by omission of MnO). For each system, the molar proportions were normalized to 100%. The anhydrous whole-rock compositions for each system are listed in Table 1. The H_2O component was added to each chemical system in the phase equilibrium modeling, in the form of excess H_2O. Fe^{3+} was not considered as a separate component in the modelling

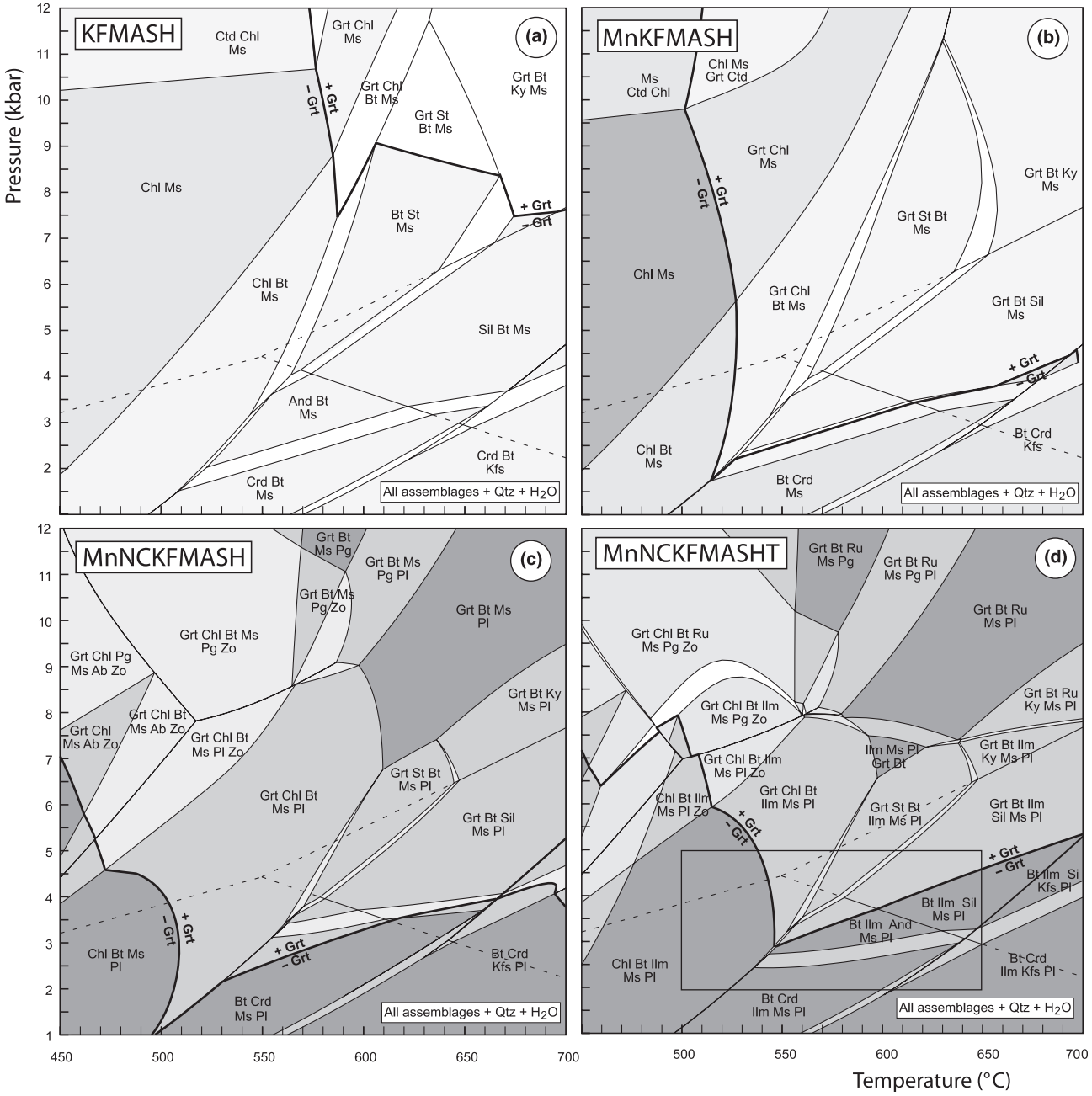

Fig. 11. Phase diagram sections for the average Nelson pelite composition in chemical systems of increasing complexity, calculated using THERMOCALC (Powell, 1998) and a modified version of the 2003 update of the Holland & Powell (1998) data base (see text for details). Abbreviations from Kretz (1983). The bulk compositions for each diagram are presented in Table 1. Increasingly darker shades of grey represent domains of increasing Gibbs phase rule variancy, starting from white = divariant. The *P*–*T* box in (d) is expanded in Fig. 12a.

Table 1. Average Nelson whole-rock compositions used for phase diagram modelling.

	Raw analysis[a] (wt%)	Raw analysis[b] (mol.%)	MnNCKFMASHT[c] (mol.%)	MnNCKFMASH[d] (mol.%)	MnKFMASH[e] (mol.%)	KFMASH[f] (mol.%)
SiO_2	60.41	68.53	69.89	71.05	71.76	71.84
TiO_2	0.93	0.80	0.81			
Al_2O_3	20.10	13.44	13.70	13.93	13.44	13.45
FeO	5.68	5.39	5.44	4.71	5.83	5.84
MnO	0.08	0.08	0.08	0.08	0.10	
MgO	2.30	3.89	3.96	4.03	4.99	4.99
CaO	1.06	1.29	1.32	1.34		
Na_2O	1.53	1.68	1.71	1.74		
K_2O	4.17	3.02	3.08	3.13	3.87	3.88
P_2O_5	0.15	0.07				
LOI	3.09					
C	0.31[a]	1.77				
S	0.027[a]	0.06				
Total	99.51	100.00	100.00	100.00	100.00	100.00

[a]Raw analysis from Pattison & Vogl (2005): C and S are part of LOI so were not added to total.
[b]Raw molar proportions, with LOI omitted but C and S included, normalized to 100%.
[c]MnNCKFMASHT: omit C and P_2O_5 from raw analysis, project from pyrrhotite, renormalize to 100%.
[d]MnNCKFMASH: as above, then project from ilmenite, renormalize to 100%.
[e]MnKFMASH: as above, then project from albite and anorthite, renormalize to 100%.
[f]KFMASH: as above, then drop MnO, renormalize to 100%.

because Fe^{3+} and Fe^{2+} were not measured separately either in the whole-rock analyses or in the mineral analyses. Most rocks in the aureole contain graphite, ilmenite and pyrrhotite, suggestive of not strongly varying, and probably low, amounts of Fe^{3+} (Connolly & Cesare, 1993). Although at pressures above the Al_2SiO_5 triple point the phase equilibria vary significantly between the different systems, in the pressure range of interest to this study (2–5 kbar) the main difference relates to the stability of garnet, and to a lesser degree the stability of cordierite *v.* andalusite.

Comparison of the garnet-in line in the four different chemical systems in Fig. 11 shows that its position is sensitive to bulk composition and possibly thermodynamic data, in contrast to the staurolite-in, andalusite-in and staurolite-out lines whose positions do not change very much from one chemical system to another. We chose the MnNCKFMASHT system for modelling the phase equilibria because it allows assessment of Mn and Ca variation in garnet, and takes account of the effect of ilmenite in sequestering some of the Fe and Mn in the rocks. Compared with the Ti-free MnNCKFMASH system, it predicts a smaller stability field of garnet, which agrees with the general absence of garnet in low-pressure cordierite-bearing rocks in the Nelson aureole and in aureoles worldwide (Pattison & Tracy, 1991). On the other hand, it is possible that the contracted garnet stability field predicted in MnNCKFMASHT, in which garnet-in occurs only 10–15 °C below staurolite-in at pressures below the triple point, is too small when one considers the lower-temperature positions of the predicted garnet-in line for individual bulk compositions from the study area (see below), and the fairly widespread development of a distinct garnet zone downgrade of the staurolite isograd in many regional facies series 2b (staurolite-andalusite-type) sequences of the same pressure as in this study (see compilation in Pattison & Tracy, 1991).

Pressure of contact metamorphism

Figure 12a is an enlargement of the part of MnNCKFMASHT phase diagram in Fig. 11d between 2 and 5 kbar and 500 and 650 °C. The sequence of mineral-in reaction isograds in Fig. 1b can be matched to the mineral-in reactions in Fig. 12a in the pressure range 3.3–4.0 kbar, over which range St + And is stable. We have chosen 3.5 kbar for subsequent modelling because of the coincidence of the staurolite and andalusite isograds in the field and the significant separation between these and the sillimanite isograd, recognizing that these could be influenced by the kinetic factors discussed below. The exact pressure does not affect the central arguments of the paper.

Temperatures of isograds

Table 2 lists the predicted temperatures of the reaction isograds along the 3.5 kbar isobaric line in Fig. 12a. The temperature ranges in Table 2 represent the minimum and maximum temperatures for each isograd reaction between 3.3 and 4.0 kbar in MnNCKFMASHT (Fig. 12a).

Figure 13a shows that even for the same chemical system, the position of the garnet-in line varies significantly for different individual rock bulk compositions. In the light of this sensitivity, we have estimated the temperature of the garnet-in reaction to be 527 °C within a range of 498–546 °C, based on the average and range of the garnet-in reaction for the different bulk compositions shown in Fig. 13a. The generally lower temperatures of the garnet-in line for the individual compositions plotted in Fig. 13a, compared with that for the average composition, may be due to their slightly Fe + Mn-richer bulk compositions.

In Fig. 14 the isograds are plotted against distance from the contact in the southern part of the aureole where there is the densest sampling (i.e. outwards from 93-CW-19 in Fig. 1b). Individual boxes in Fig. 14 correspond to a distance uncertainty of ± 25 m and a temperature uncertainty corresponding to the temperature range in Table 2, with the solid dots in the boxes being the temperature estimate for 3.5 kbar. Absolute temperature uncertainties, arising from uncertainties in the thermodynamic data, activity–composition relations of the minerals, and possible deficiencies in the choice of chemical system for the modelling (e.g. no consideration of Fe^{3+}), are likely larger than the temperature ranges in Table 2, but are difficult to quantify (see Waters & Lovegrove, 2002 and Powell & Holland, 2008 for detailed discussions). However,

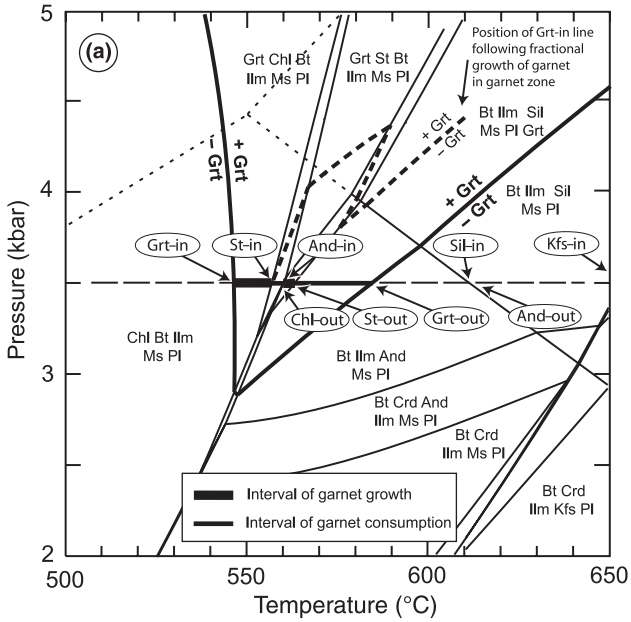

Fig. 12. (a) *P–T* phase diagram section for average Nelson pelite in the system MnNCKFMASHT (see Fig. 11d and text). Labels in the ellipses are for mineral-in and mineral-out reactions interpreted to correspond to the isograd reactions in Fig. 1b. Intervals of predicted garnet growth and consumption along the inferred isobaric 3.5 kbar isobaric *P–T* path are indicated by thick and thinner solid lines, respectively. (b, c) Changes in predicted mole fractions of phases, normalized to a sum of one molar oxide in each phase (~ mineral modes), going upgrade along the isobaric 3.5 kbar *P–T* path in (a).

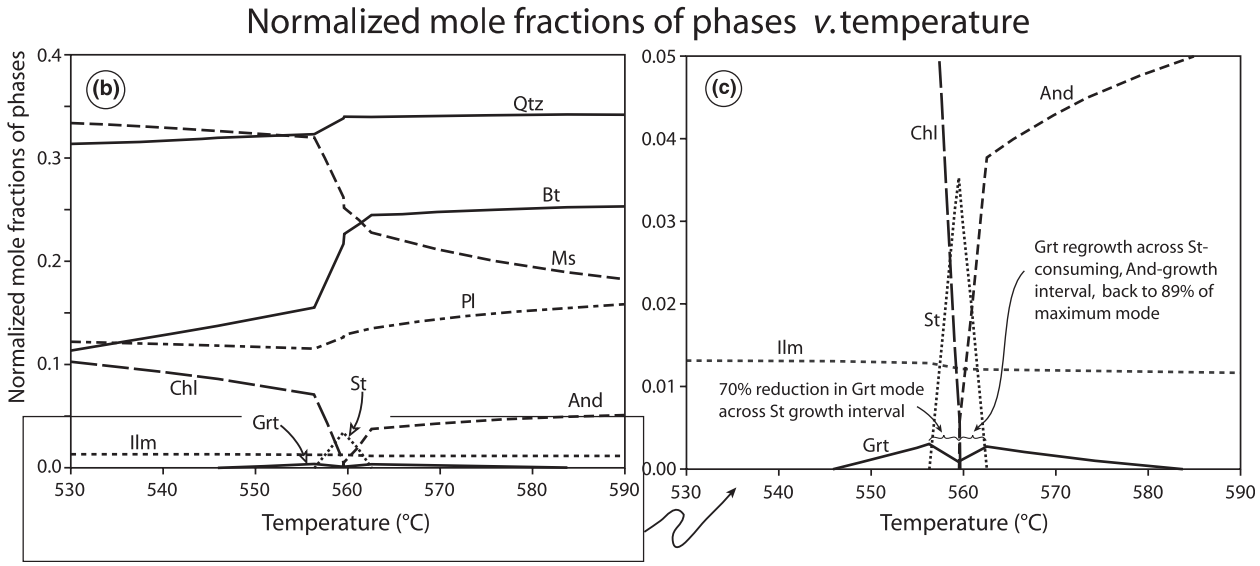

Table 2. Temperatures and distances of isograds from the contact.

	Distance from contact[a] (±25 m)	Temperature[b] (°C)	Temp. range[c] (°C)
Grt-in	1400	527[d]	498–546[d]
St-in	1340	557	553–563
And-in	1340	560	553–578
Sil-in	390	611	578–630
Major St-out, Sil-in	290	563	556–583
St-relics out	200	563	556–583
And-out	130	611	578–630
Kfs-in	70	653	646–668

[a]Measured outwards from 93-CW-19 in Fig. 1b.
[b]Temperatures of isograds at 3.5 kbar for MnNCKFMASHT.
[c]Temperature range of isograds between 3.3 and 4.0 kbar for MnNCKFMASHT.
[d]Average and range of Grt-in line for different bulk compositions and chemical systems for 3.5 kbar (see text for discussion).

relative uncertainties are unlikely to be much greater than those listed in Table 2 when one considers the consistency of facies series 2b isograd sequences worldwide and the small predicted temperature separation (10–40 °C) between the isograd reactions (Pattison & Tracy, 1991).

THERMAL MODELLING

Figure 14 shows a thermal profile for the aureole (maximum temperature *v.* distance from the contact), calculated using the one-dimensional thermal modelling software of Peacock (1990). The tabular shape of the tail of the Nelson batholith adjacent to the study area (Fig. 1a) makes this simple modelling appropriate. The parameters used in the construction of the

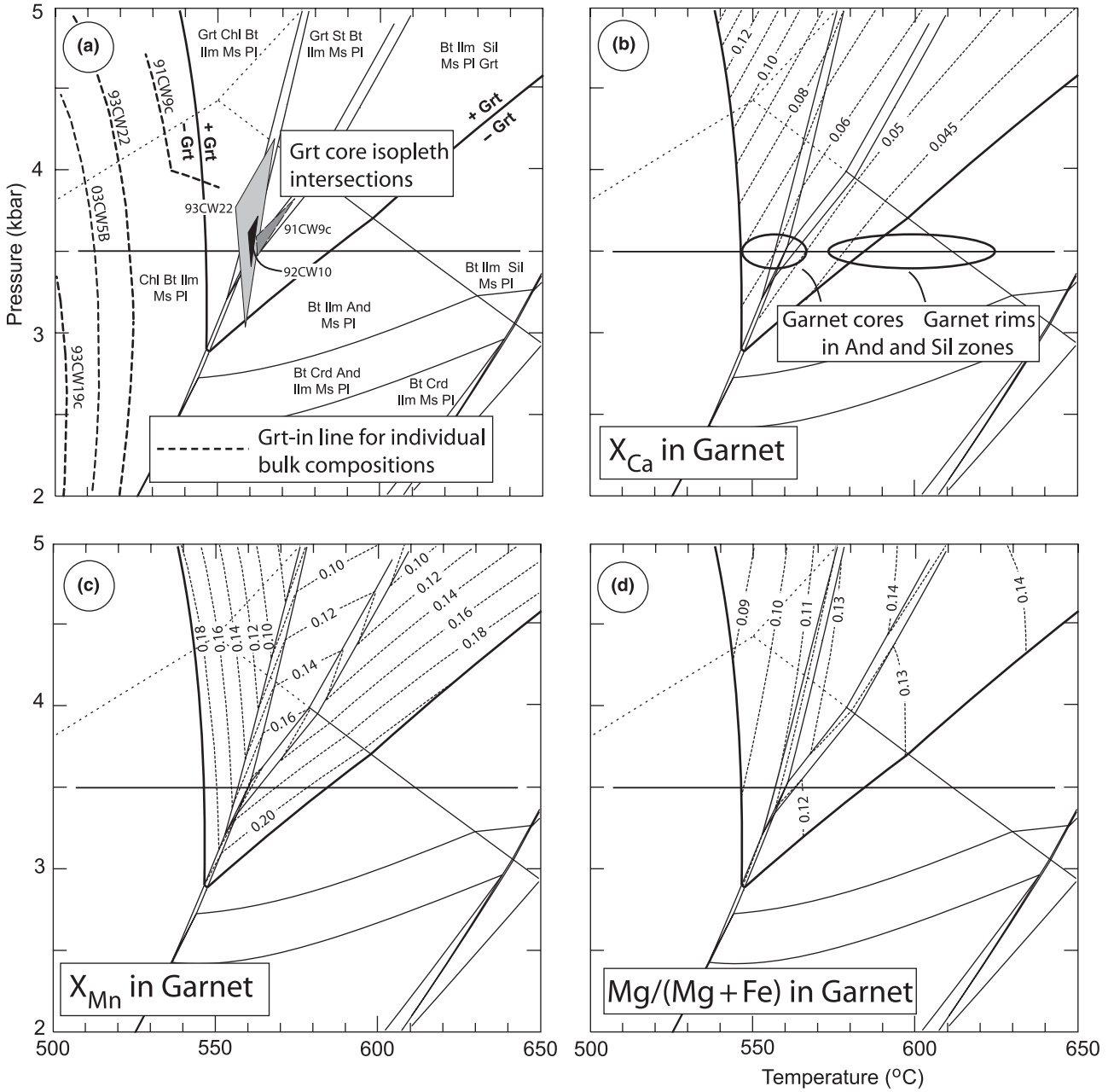

Fig. 13. (a) *P–T* equilibrium phase diagram section (same as in Fig. 12a) showing positions of garnet-in lines for bulk compositions of individual rocks, and garnet–core–isopleth intersections for individual rocks whose garnet have values of X_{Mn}^{Grt} that occur within the range in (c) (see text for discussion). (b) Calculated isopleths of X_{Ca}^{Grt}, and range of measured X_{Ca}^{Grt} in garnet cores and rims from rocks in the andalusite and sillimanite zones. (c) Calculated isopleths of X_{Mn}^{Grt}. (d) Calculated isopleths of $Mg/(Mg+Fe)^{Grt}$.

profile are given in the caption to Fig. 14, based on *a priori* estimates of thermal and spatial parameters pertinent to the Nelson intrusion and country rocks.

The calculated thermal profile in Fig. 14 is nevertheless non-unique and can vary substantially when one or more of the several poorly constrained input parameters are varied, including some not incorporated in Peacock's modelling such as the effect of endothermic metamorphic reactions. On the other hand, all calculated profiles have the same form as the one in Fig. 14, so that comparison of the observed locations of the isograds with this profile reveals important first-order features that are independent of the details of the thermal modelling. The profile shown in Fig. 14 is consistent with minimal overstepping of the muscovite-out/K-feldspar-in and chlorite-out/andalusite-in reaction isograds, a prediction that is discussed further below.

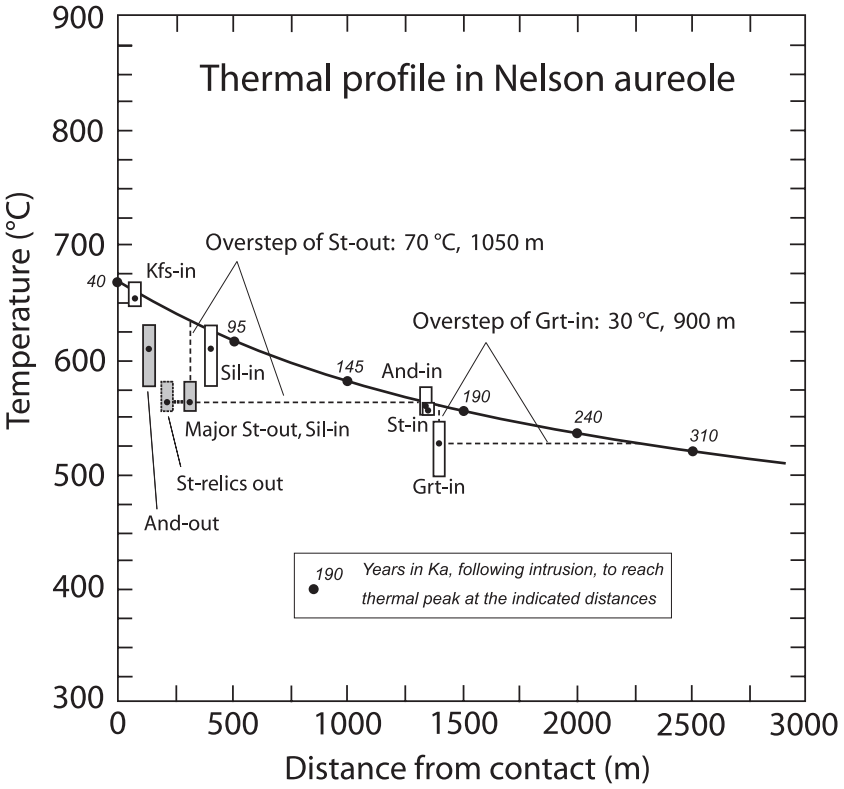

Fig. 14. Comparison of modelled thermal profile in the Nelson aureole (solid line) with the observed locations of isograds and their temperatures assuming equilibrium (boxes with dots). For the thermal modelling, the software of Peacock (1990) was used, with the following parameters: ½ width of tabular intrrusion: 1750 m. *T* of country rock at time of intrusion: 400 °C. *T* of magma: 900 °C. *T* of crystallization interval: 200 °C. Enthalpy of crystallization: 100 kJ kg^{-1}. Thermal conductivity: 2.25 W m K^{-1}. Heat capacity of solids: 1000 J kg K^{-1}. Density of solids: 2.75 kg m^{-3}. Time step: 500 a. Number of time steps: 2000. Total time elapsed in simulation: 1 Myr. For the isograd locations, the dots and boxes represent the mean and range of the equilibrium isograd temperatures combined with a distance uncertainty of ±25 m (data in Table 2).

COMPARISON OF PREDICTED PHASE EQUILIBRIA WITH OBSERVATIONS

The following section compares the observed features of the prograde metamorphic sequence in the Nelson aureole with the thermodynamically predicted features. This approach involves several assumptions. First, chemical equilibrium is assumed. Studies such as Carlson (2002) have provided evidence for thin section-scale chemical disequilibrium during garnet growth, especially involving Ca and some trace elements, which they ascribed to the kinetics of intergranular diffusion. For this reason, we only focus on major features of composition and chemical zoning that can be plausibly related to reactions involving the rock-forming minerals. Preserved growth zoning in garnet and general lack of garnet dissolution indicates that prograde fractional crystallization has occurred. Whereas modelling of prograde fractional crystallization of garnet, discussed later in the paper, results in significant contraction of garnet stability compared with the equilibrium model, it has relatively little effect on other phase boundaries or on mineral composition isopleths, most likely because of the minor amounts of garnet (< 1 vol.%) that are predicted to be formed.

Second, it is assumed that the reaction isograd temperatures are close to those calculated in Figs 12 and 13 and Table 2, acknowledging that there is uncertainty in the absolute and relative temperatures due to the factors discussed above, and to the assumed pressure of contact metamorphism. For example, assuming a pressure of 3.8 kbar rather than 3.5 kbar results in a larger predicted temperature separation between the staurolite-in and andalusite-in reactions (15 °C *v.* 3 °C), and a smaller predicted temperature separation between the andalusite-in and sillimanite-in reactions (20 °C *v.* 50 °C). The greatest uncertainty is on the temperature of the garnet-in reaction. Although it could be argued that, within the uncertainties of the calculations, there is no significant temperature difference between the garnet-in and staurolite-in reactions, the common textural evidence for early garnet growth in the Nelson rocks, and the abundance of prograde sequences of the same pressure as the Nelson aureole that do contain a significant garnet zone downgrade of the staurolite zone (Pattison & Tracy, 1991), suggest that there is a significant temperature difference between them. In the interpretations that follow, the consequences of varying the temperature of the garnet-in reaction are discussed.

Third, we assume that a_{H2O} was unity during progress of the prograde reactions, even though the rocks are graphitic. Assuming the graphitic metapelites were not pervasively infiltrated with fluid during intervals of reaction, when they were internally generating and expelling their own H_2O, a_{H2O} will have been internally buffered by graphite to values of ~0.85–0.95 (Connolly & Cesare, 1993). The result is an overall lowering by 10–15 °C of the absolute positions of the dehydration reactions in Table 2, but

an insignificant change in the temperature differences among them (Pattison, 2006).

Mineral-in isograds

The predicted order of mineral growth in Fig. 12a agrees with the porphyroblast textures (Figs 2–10), in which garnet occurs as inclusions in all porphyroblasts and staurolite occurs as inclusions in andalusite, with the opposite relations never observed. A caveat to this interpretation is that such enclosing relationships show the relative timing of the end of growth of porphyroblasts rather than the beginning of their growth (e.g. Vernon & Powell, 1976), such that it is possible that larger porphyroblasts such as staurolite or andalusite could enclose smaller, possibly later-nucleating, phases like garnet. We nevertheless favour the first interpretation because of the consistency of these enclosing relationships in the Nelson aureole and in other facies series 2b (staurolite-andalusite) settings worldwide (Pattison & Tracy, 1991).

On the other hand, the predicted spacing of the mineral-in isograds does not agree with the observed spacing (compare Figs 1b, 12a & 14). In the field, the garnet, staurolite and andalusite isograds are almost coincident (Fig. 1b), even though the garnet-in reaction is predicted to occur ~30 °C below the staurolite- and andalusite-in reactions (Table 2). A drop of 30 °C from conditions of the staurolite-in isograd equates to about 900 m in distance (Fig. 14). When the temperature uncertainty on the garnet-in isograd is taken into account, this distance ranges between ~250 m and ~2000 m. Figure 15 compares the mapped position of the isograds from Fig. 1b with the predicted position of the isograds based on the thermal profile in Fig. 14 and assuming that the reactions proceeded at equilibrium along the 3.5 kbar isobaric line in Fig. 12a. Figure 15 shows that there is potentially a substantial domain in the field downgrade of the observed garnet isograd where garnet should have grown according to equilibrium predictions.

The spatial coincidence of the staurolite-in and andalusite-in isograds in Fig. 1b is consistent with the small predicted separation between the isograd reactions of < 5 °C (Fig. 12a and Table 2), acknowledging the possibility that the two reactions could have been more separated in temperature but proceeded together because of kinetic factors. The sillimanite-in isograd occurs ~20 °C and 250 m upgrade of where it is predicted to occur in Fig. 14. As noted above, the initial

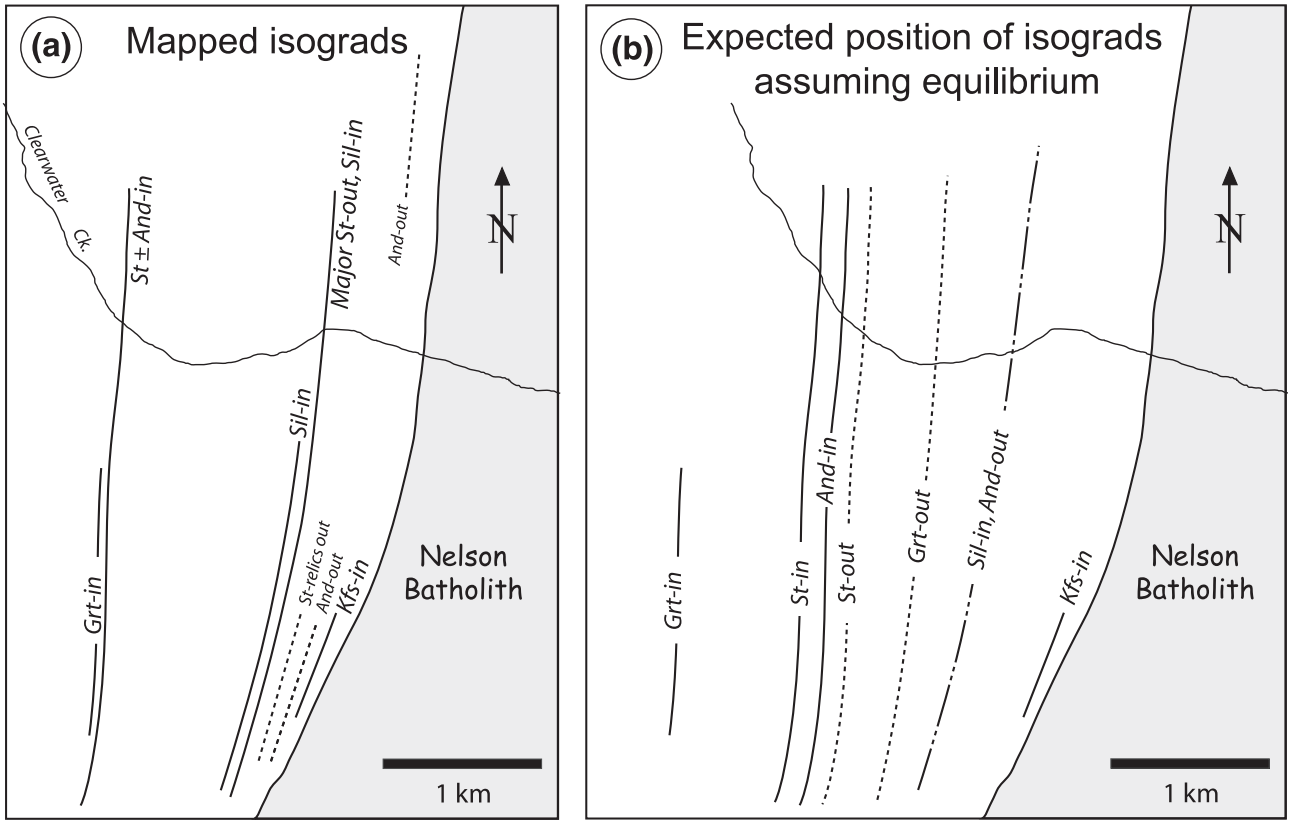

Fig. 15. Comparison of observed isograd locations with predicted locations assuming equilibrium. (a) Observed isograds from Fig. 1b. (b) Predicted positions, based on temperatures in Table 2 and distances corresponding to those temperatures from the thermal profile in Fig. 14.

development of sillimanite involves small amounts of fine-grained and fibrolitic sillimanite, and appears to be due to localized reaction involving matrix minerals rather than whole-rock reactions. The major sillimanite-forming reaction, associated with major consumption of staurolite, is discussed below.

Mineral-out isograds

The predicted sequence and spacing of mineral-out isograds do not match the observations at all. Garnet is ubiquitous at all grades and shows little evidence for consumption, even though it is predicted to dissolve significantly during staurolite production and to be completely consumed downgrade of the Kfs + Sil isograd by the continuous reaction:

$$\mathrm{Ms} + \mathrm{Grt} = \mathrm{And} + \mathrm{Bt} + \mathrm{Qtz}. \quad (9)$$

The major staurolite-out, sillimanite-in isograd occurs ~1050 m upgrade of where staurolite is predicted to have reacted out, corresponding to a temperature overstep of ~70 °C. Staurolite relics persist at even higher grade. In contrast, there is evidence for patchy reaction of staurolite to andalusite throughout the 1100 m interval between the staurolite + andalusite isograd and the major staurolite-out, sillimanite-in isograd (Figs 1b & 3).

The andalusite-out isograd occurs 500 m above the predicted andalusite-out reaction, corresponding to a temperature overstep of ~45 °C. Whereas the metastable persistence of andalusite into the sillimanite zone is well known in other contact aureoles (see Pattison & Tracy, 1991 for a review), the unreactive behaviour of garnet and staurolite is less commonly noted.

Textures and chemical zoning of garnet

The isobaric *P–T* path through Fig. 12a predicts intervals of garnet growth and dissolution for the average Nelson pelite composition that can be compared with the observed textures and chemical zoning of garnet in the aureole. In addition to the general caveats noted above, this approach fails in detail because small differences in bulk composition between individual rocks and the modelled average composition in Fig. 12a, including in minor elements such as Ca, Mn and P, can have a significant effect on the stability and composition of the garnet. Nevertheless, in all models, garnet is predicted to undergo two intervals of growth and two intervals of consumption during prograde metamorphism (Fig. 12a), the last leading to complete consumption in the andalusite zone by reaction (9) (for some individual bulk compositions, final garnet consumption occurred in the sillimanite field). Predicted changes in mole fractions of phases along the 3.5 kbar isobaric path, normalized to a sum of one molar oxide in each phase (and therefore a good approximation to modal changes), are provided

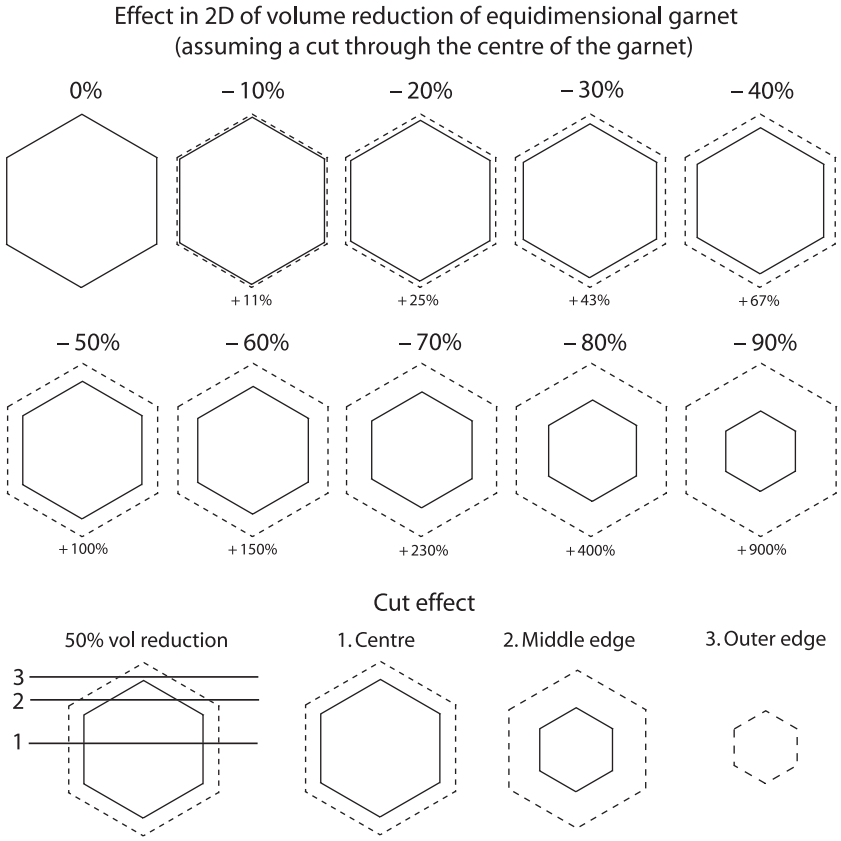

Fig. 16. Area *v.* volume in porphyroblast size reduction, assuming an equidimensional porphyroblast such as garnet. The large numbers above each frame are per cent volume reduction going from the outer dashed outline to the inner solid outline, whereas the small numbers beneath each frame are per cent volume increase going from the inner solid outline to the outer dashed outline.

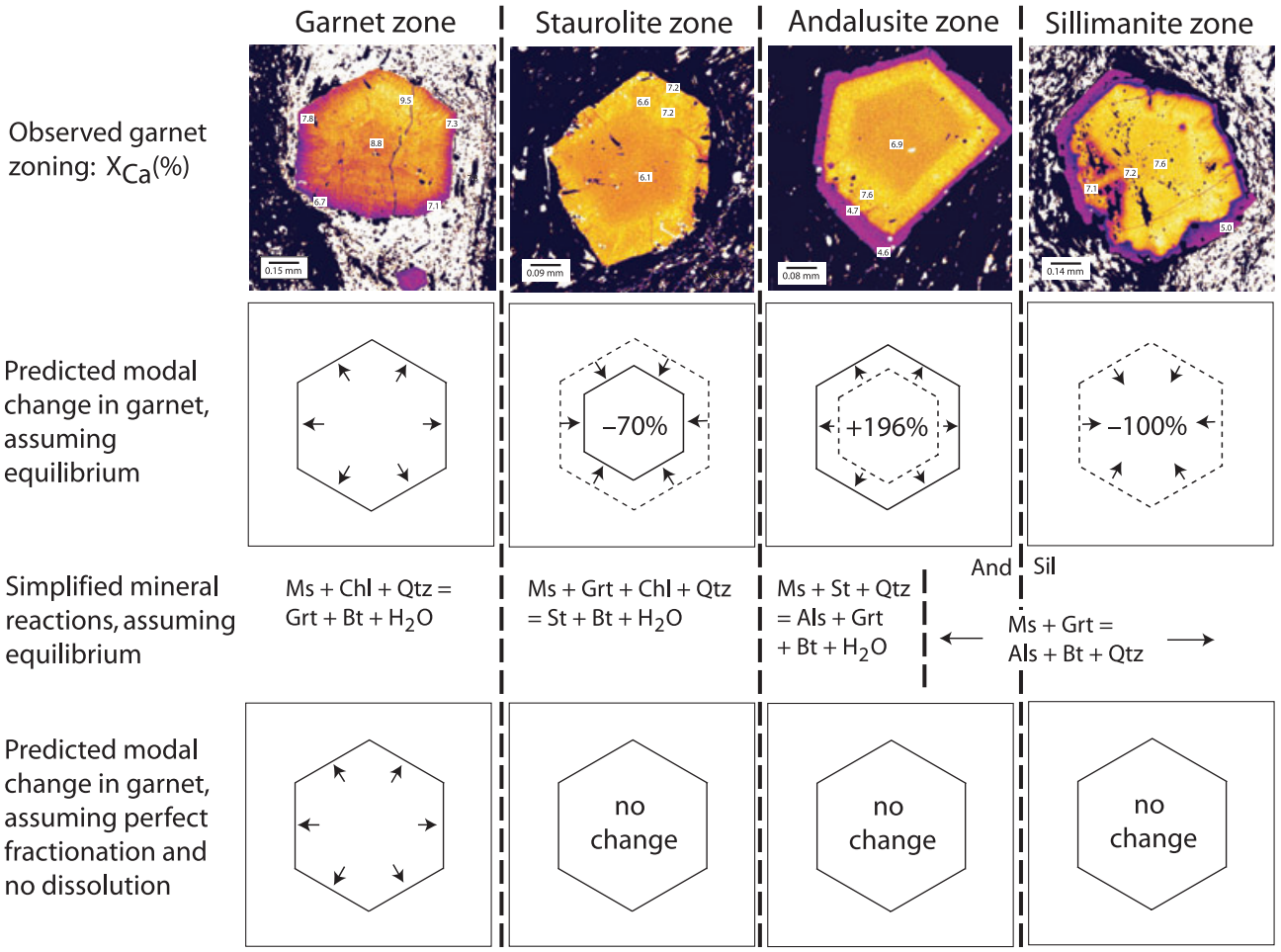

Fig. 17. Comparison of texture and calcium zoning of garnet (top row), with predicted garnet growth and consumption for two end-member models: equilibrium (second row), and perfect fractional growth of garnet with no dissolution (bottom row). Simplified mineral reactions for the equilibrium model, based on Fig. 12, are listed beneath the second row. See text for discussion.

in Fig. 12b,c. Calculated isopleths of X_{Ca}^{Grt}, X_{Mn}^{Grt} and $Mg/(Mg+Fe)^{Grt}$ for the average pelite composition are shown in Fig. 13b–d, and isopleth intersections for garnet cores from three samples whose X_{Mn}^{Grt} fall within the range in Fig. 13c, are shown in Fig. 13a.

Comparison of predicted modal changes with what is observed in the rocks requires a quantitative estimate of the extent of garnet dissolution or growth from petrography. This is difficult because a thin section is a two-dimensional slice through a three-dimensional object, so that significant volume reductions may result in only small reductions in area. The problem is illustrated in Fig. 16, in which volume reductions of up to about 20% may be difficult to detect. Figure 16 also shows that cut effects must be considered. In contrast to the euhedral resorbed products illustrated in Fig. 16, dissolution is unlikely to proceed evenly on all sides of a porphyroblast, instead being focused at corners and edges of crystals, and in domains of enhanced reactivity. Figure 17 shows a comparison of zoning in X_{Ca}^{Grt} from the garnet, staurolite, andalusite and sillimanite zones with predicted garnet growth and consumption from phase equilibrium modelling, in which modal changes are assessed with reference to Fig. 16.

Garnet zone

Garnet growth is predicted over a ~30 °C interval downgrade of the first development of staurolite. Extending the garnet isopleths in Fig. 13b–d to the inferred temperature of 527 °C at 3.5 kbar for the onset of garnet growth (~25 °C below the garnet-in line shown in Figs 12 & 13), X_{Ca}^{Grt} is predicted to smoothly decrease from 0.09 to 0.06 through this garnet growth interval, ignoring minor fractional effects. Euhedral chemical zoning in garnet from the garnet zone (Figs 4 & 5), and in the inner portions of garnet from the staurolite, andalusite and sillimanite zones (Figs 6–9), is consistent with progressive growth of garnet, but in contrast to the steadily decreasing values of X_{Ca}^{Grt} predicted in Fig. 13b, the oscillatory

and flame-like Ca zoning indicates more complex processes. The concentric Ca zoning could indicate involvement of minor Ca-bearing phases like epidote and allanite that are not predicted to be present in Fig. 12a, but which are observed in the rocks. This possibility is further suggested by the Y zoning, which Tomkins & Pattison (2007) argued reflected successive consumption of xenotime and allanite during garnet growth, the latter producing monazite. The range of observed values of X_{Ca}^{Grt} in the garnet centres (0.05 to 0.07, neglecting the anomalously Ca + Mn-rich garnet in 03CW05) is lower than predicted by equilibrium modelling. This discrepancy could be ascribed to a number of factors, such as errors in the thermodynamic data or small differences between the model bulk composition and the bulk composition of the individual rocks containing the analysed garnet. On the other hand, the clustering of garnet core isopleth intersections around the staurolite-in reaction in Fig. 13a is consistent with the close coincidence of the garnet, staurolite and andalusite isograds in the field, and could be accounted for by delayed garnet growth.

Staurolite zone

Approximately 70% of the garnet that grew in the garnet zone is predicted to be consumed in the production of staurolite (Fig. 12c). The euhedral external shape and internal chemical zoning of garnet in the staurolite zone (Figs 6 & 7) argues against significant resorption, although there is some evidence for rounding of corners of some garnet crystals. Comparison with Fig. 16 suggests that it is unlikely that there was more than about 10% garnet resorption during staurolite growth, and possibly none at all in some rocks.

Andalusite zone

Figure 12c predicts a second interval of garnet growth accompanying andalusite growth and staurolite consumption, such that it attains 89% of its maximum predicted mode immediately prior to staurolite growth. Evidence in support of a second interval of garnet growth is the low-Ca rim that occurs on the margin of garnet grains in andalusite-bearing rocks (Figs 8 & 17). The width of the low-Ca outer rims in Fig. 8, assuming near-centre cuts through the garnet and with reference to Fig. 16, suggests 40–70% increase in garnet volume accompanying development of andalusite, much less than the ~200% growth predicted in Figs 12c & 17. The X_{Ca}^{Grt} of the rims is 0.02–0.03 lower than the garnet on which the rims grew, a difference that is significantly greater than the very small differences predicted in Fig. 13b. Assuming that andalusite growth occurred primarily due to staurolite breakdown, the lower than predicted X_{Ca}^{Grt} is consistent with the kinetically delayed staurolite breakdown to andalusite noted earlier, in which the garnet that grew as part of this reaction inherited a composition reflecting the higher temperatures of the kinetically delayed reaction.

Sillimanite zone

Garnet is predicted to be consumed in the andalusite zone (Fig. 12). However, garnet in sillimanite zone rocks (e.g. Fig. 9) has low-Ca rims that contain sillimanite needles, indicating garnet *growth* in the sillimanite field. As above, the most likely explanation is metastable persistence of staurolite into the stability field of sillimanite, at which point it reacted to form sillimanite and low-Ca garnet (i.e. the staurolite-out, major sillimanite-in isograd in Figs 1b & 14). The low-Ca rims of garnet in Fig. 9 show a somewhat irregular margin on their inner edge, suggesting dissolution prior to growth of the rim, possibly in association with staurolite growth by reaction (2), or through reaction (9).

K-feldspar zone

Garnet in this zone contains a relatively high-Ca core mantled by a low-Ca rim, like that seen in the andalusite and sillimanite zones, but contains in addition an outer low-Ca rim, separated from the inner low-Ca rim by a euhedral Y annulus (Fig. 10). Sillimanite needles occur in the outer rim. Assuming that the core and inner low-Ca rim grew in a similar manner to that in the andalusite and sillimanite zones, the outermost low-Ca rim is ascribed to garnet growth during or following the reaction of muscovite to form sillimanite and K-feldspar. By analogy with the study of Pyle & Spear (2003), the Y annulus may reflect garnet growth in the presence of a melt phase, consistent with the migmatitic textures in the rocks (Pattison & Vogl, 2005). In general, the Ca zoning in the sillimanite and K-feldspar zones shows more evidence for garnet dissolution than in the staurolite and andalusite zones, most likely due to higher absolute temperatures.

INTERPRETATION OF DISCREPANCIES BETWEEN EQUILIBRIUM MODELLING AND OBSERVATIONS

The major discrepancies between the observations and phase equilibrium predictions include the:
1 relative unreactivity of garnet going upgrade;
2 close proximity of the garnet-in, staurolite-in and andalusite-in isograds;
3 patchy progress of the staurolite-consuming, andalusite-producing reaction; and
4 relatively abrupt disappearance of staurolite once sillimanite develops.

Unreactivity of garnet

The observations above suggest that garnet grew in intervals in which it was a reaction product but did

not dissolve as much as predicted when it was a reactant. We therefore tested a scenario in which garnet is modelled to undergo perfect prograde fractional crystallization during periods of predicted growth, but not to dissolve at all during periods of predicted dissolution. The fractional crystallization calculations utilized the program THERMOCALC and were calculated using the predicted garnet mode and composition to modify the whole-rock composition in one-degree increments to account for growing garnet.

The calculated modal behaviour of garnet in the two models is shown in Fig. 17. In the fractional growth model, the bulk rock becomes impoverished in elements that fractionate into garnet, in particular Mn, driving the system closer to the Mn-free NCKFMASHT system as garnet grows. The effect is to displace the garnet-in line continuously up-temperature and up-pressure as garnet grows, and concomitantly, but to a much lesser degree, the position of the isopleths. The displaced garnet-in line for the fractionated bulk composition at the point that staurolite begins to grow is shown as dashed lines in Fig. 12a. An interesting feature in this model is that garnet is not predicted to grow at all upgrade of the garnet zone (the garnet-in isopleth lies above 3.5 kbar).

Comparison of the predicted behaviour of garnet with the observed garnet textures and chemical zoning in Fig. 17 suggests that neither of the equilibrium nor fractional growth/no dissolution end-member models satisfies the observations. There is substantially less garnet dissolution in the staurolite zone than predicted by the equilibrium model but more garnet growth in the andalusite zone than predicted by the fractional growth/no dissolution model. The natural process may lie somewhere between these end-members. On the other hand, garnet growth in the sillimanite zone is predicted by neither model, and is most likely due to the kinetic delay in the staurolite-consuming, sillimanite + garnet-producing reaction, resulting in metastable garnet growth at higher temperatures.

Reaction overstepping and reaction affinity

As noted above, several reactions in the aureole appear to have been overstepped in temperature. A primary determinant of the extent to which a reaction is overstepped due to kinetic barriers is the reaction affinity (see Introduction). Reaction affinity in thermally overstepped reactions is related to the entropy difference (ΔS) between the thermodynamically stable, but not yet crystallized, equilibrium assemblage, and the metastable reactants, by the equation $A = \Delta T * \Delta S$, where ΔS is as defined above and ΔT is the temperature overstep of the equilibrium boundary ($= T - T_{eq}$). For the prograde reactions of concern to this study, $T > T_{eq}$.

Calculating reaction affinity in natural systems is an inexact exercise because the nature of the compositional departures of reactant and product phases from equilibrium cannot be predicted. Some reactant phases may change composition as the reaction is overstepped whereas others may not, and the compositions of product minerals that do finally nucleate and grow are unknown other than within limits.

We therefore follow the approach of Walther & Wood (1984), Lasaga (1986) and Waters & Lovegrove (2002), who calculated reaction affinities for simplified end-member reactions that provide an approximation to the more complex reactions that actually proceeded in the rocks. Using this approach, the above equation becomes $A = \Delta T * \Delta_r S_{P,T}$, where $\Delta_r S_{P,T}$ is the entropy change of the model reaction.

Table 3 lists entropy changes for the model reactions relevant to this study. With one exception, the entropy changes were calculated at 3.5 kbar, 560 °C, the equilibrium temperature of the staurolite-forming reaction. The entropy change of the sillimanite + K-feldspar reaction entropy was calculated at 3.5 kbar, 650 °C. The thermodynamic data of Holland & Powell (1998, 2003) were used. The entropy values in Table 3 are the mean of the values for the Fe- and Mg-end-member reactions, normalized per mole of oxygen in the porphyroblast phase to allow comparison between reactions (Waters & Lovegrove, 2002). The normalized

Table 3. Entropies of reaction.

Reaction number in text	Reaction label	Simplified reaction in KFASH or KMASH	No. oxygens in porphyroblast	Normalized moles H_2O[a]	Normalized $\Delta_r S_{P,T}$[b]	Width of Fe-Mg divariant interval in °C
1	Grt-in	1Ms + 3Chl + 3Qtz = 4**Grt** + 1Bt + 12H_2O	Grt: 12	0.25	16.1	40
3	St-in	41Ms + 31Chl = 8**St** + 41Bt + 33Qtz + 108H_2O	St: 48	0.28	17.0	3
5	And-in (from Chl)	5Ms + 3Chl = 8**And** + 5Bt + 1Qtz + 12H_2O	And: 5	0.30	19.1	2
4	And-in (from St)	8Ms + 6St + 17Qtz = 62**And** + 8Bt + 12H_2O	And: 5	0.04	3.6	5
9	Grt-out	Ms + **Grt** = 2And + Bt + Qtz	Grt: 12	0.00	0.6[c]	> 50
7	Sil-in (from And)	And = **Sil**	Sil: 5	0.00	0.6	0
8	Sil + Kfs-in	Ms + Qtz = **Sil** + Kfs + H_2O	Sil: 5	0.20	14.2	0

[a]Moles H_2O in reaction, per mole of O in indicated product or reactant porphyroblast.
[b]J K^{-1} per mole of O in indicated product or reactant porphyroblast.
[c]KFASH estimate.

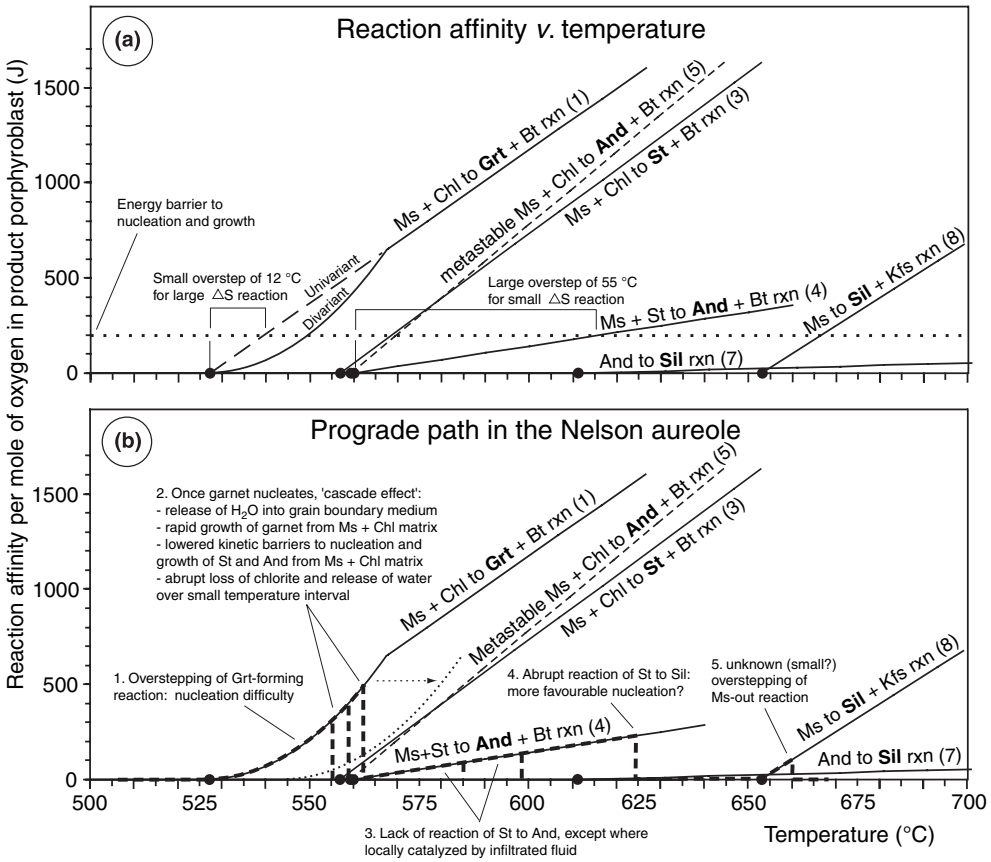

Fig. 18. (a) Reaction affinity *v.* temperature for reactions in the Nelson aureole. Slopes of reactions are calculated from entropy data in Table 3, with the exception of the curved part of garnet-forming reaction (1), which is discussed in the text. The equilibrium positions of reactions (intercepts along horizontal axis, corresponding to zero reaction affinity) come from Fig. 12a and Table 2. The dotted line for energy barrier to nucleation and growth is representative only. See text for further discussion. (b) Representative prograde path that accounts for many of the features observed in the Nelson aureole. The dotted arrow and curve for reaction (1) are discussed in the text.

number of moles of H_2O produced in each reaction is also listed, from which can be seen the strong correlation between entropy of reaction and moles of H_2O produced.

Reaction affinities were calculated using the equation $A = \Delta T * \Delta_r S_{P,T}$. A complication in applying the values in Table 3 to the real reactions in the rocks is the effect of multivariancy (for example, in KFMASH, Fe-Mg divariancy). Whereas the Sil + Kfs-producing reaction (7) is univariant, giving rise to a simple linear increase in reaction affinity with degree of temperature overstep, the Fe-Mg reactions in Table 3 are divariant. In an equilibrium model, the extent of reaction going up-temperature through a divariant interval increases from 0% at the temperature at which the reaction interval is entered to 100% at the temperature at which the reaction interval is exited. The entropy change at any given temperature in a divariant interval is therefore the product of the end-member (or 'full') entropy change listed in Table 3 and the predicted extent of reaction at that temperature. Reaction affinity, the product of the temperature overstep and the predicted entropy change, therefore increases nonlinearly going though the reaction interval, becoming linear thereafter.

Reaction affinity *v.* temperature for the reactions encountered going upgrade along an isobaric *P-T* path at 3.5 kbar is illustrated in Fig. 18a. The temperatures of each reaction at zero reaction affinity (i.e. at equilibrium) are given in Fig. 12a and Table 2. Metastable reaction (5), involving growth of andalusite from Ms + Chl, is shown as a dashed line. For most of the reactions in Table 3, the width of the multivariant reaction interval is < 5 °C and so is ignored for the purposes of this study. For garnet-forming reaction (1), however, the multivariant interval is $\sim$40 °C, based on calculations in KFMASH for a bulk-rock Mg/(Mg + Fe) corresponding to the average pelite. The curvature of reaction (1) in Fig. 18a going through the divariant interval results in significantly lower reaction affinity at small temperature oversteps (e.g. < 20 °C) compared with the situation in which the multivariancy of reaction (1) is ignored (linear dashed line in Fig. 18a). A general feature of Fig. 18a is that,

for a given reaction affinity needed to overcome barriers to nucleation and growth, reactions with high $\Delta_r S_{P,T}$ achieve this after a smaller temperature overstep than reactions with low $\Delta_r S_{P,T}$.

Overstepping of garnet formation

The near coincidence of the garnet-in isograd with the staurolite-in and andalusite-in isograds, and the clustering of garnet core isopleth intersections around the staurolite-in reaction in Fig. 13a are consistent with overstepping of the garnet-forming reaction. Overstepping is expected to result in a relatively rapid growth of garnet, consistent with the textural and chemical zoning features in garnet noted above.

The magnitude of the overstep in energy needed to nucleate and grow garnet can be estimated from Fig. 18b. Delay in the onset of the garnet-forming reaction to the temperature of the staurolite isograd (~30 °C) corresponds to a reaction affinity of ~400 J per mole of oxygen in garnet, equivalent to ~4.8 kJ per mole of garnet or ~1.6 kJ per mole of H_2O released in the reaction. As noted by Waters & Lovegrove (2002), these values correspond to the lower end of the range of 1–10 kJ per mole of H_2O deduced by Ridley & Thompson (1986) in their comparison of seeded and unseeded phase equilibrium experiments, and are comparable with the estimates of Wilbur & Ague (2006) from crystal growth simulations. On the other hand, if the equilibrium position of the garnet-in reaction occurs only 10–15 °C below the staurolite-in reaction, such as modelled in Figs 12 & 13, the predicted reaction affinity due to thermal overstepping is much lower (< 100 J per mole O in garnet) because of the shallowing slope of reaction (1) in Fig. 18b with decreasing temperature overstep (dotted line in Fig. 18b).

The most likely cause of the delay in garnet formation was difficulty of garnet nucleation. Once the activation energy barriers were finally overcome and initial garnet growth commenced, hydrous fluid accompanying garnet growth would have entered the grain boundaries. This in turn would have lowered the kinetic barriers to nucleation and growth, leading to an abrupt increase in reaction progress and potentially rapid garnet growth.

Processes at the staurolite-in and andalusite-in isograds

In addition to the near coincidence of the garnet, staurolite and andalusite isograds, the lack of evidence for involvement of garnet in staurolite formation and of staurolite in andalusite formation near the isograds suggests that all three porphyroblasts grew from reaction of matrix chlorite and muscovite over a small temperature interval.

There are at least two possible explanations for this observation. The first is a 'cascade effect', in which the release of fluid into the intergranular domain accompanying the initial formation of garnet may have abruptly lowered activation energy barriers for nucleation and growth of staurolite and andalusite as well. The cascade effect suggested here is somewhat different from that described by Waters & Lovegrove (2002), in which nucleation of a phase (e.g. staurolite) up-temperature of where it was predicted to form allowed several reactions, both stable and metastable, to contribute to its growth, resulting in an interval of vigorous reaction. The fluid-related cascade effect suggested here may have allowed several Ms + Chl-consuming reactions to proceed in parallel. Growth of garnet, staurolite and andalusite from the same Ms + Chl substrate would imply that the garnet-, staurolite- and andalusite-forming reactions were all overstepped to some degree. The relative progress of the competing reactions would then be determined by the interplay between the kinetics of each reaction and the overall tendency to minimize the free energy of the system.

Such overstepping opens the possibility of out-of-order mineral growth, as documented in the Bushveld aureole by Waters & Lovegrove (2002) and in the Ubehebe aureole by Muller *et al.* (2004). For the Nelson aureole, we interpret the textural evidence to indicate sequential growth of garnet, staurolite and andalusite in the order predicted in the equilibrium phase diagram. Therefore a second possible explanation is progressive fractional growth of each porphyroblast mineral from the Ms + Chl matrix without significant dissolution of the earlier-formed porphyroblasts, resulting in a progressively chlorite-poorer, Mg-richer reactant matrix composition. The predicted effect of this fractionation process (see fig. 12e of Pattison & Vogl, 2005) would be sequential growth of garnet, staurolite and andalusite. Depending on its initial abundance, loss of chlorite during progressive fractionation would result in the development of Grt-, Grt + St-, and Grt + St + And-bearing assemblages, as observed (Fig. 1b). Fe(± Mn)-poorer rocks may have resulted in sequential growth of staurolite and andalusite with no garnet, also as observed. The lack of consumption of garnet during staurolite growth, and of staurolite during andalusite growth, may be ascribed to sluggish porphyroblast dissolution compared with the vigorous matrix reaction and porphyroblast growth in this narrow temperature interval.

A combination of both processes may be the best explanation for the observations. In any scenario, the compressed garnet, staurolite and andalusite isograds represent a narrow temperature interval over which chlorite reacted out of the rocks. The relatively abrupt disappearance of chlorite may be accounted for by a combination of a relatively steep increase in reaction affinity as the chlorite dehydration reactions were overstepped, and reaction acceleration due to internal generation of fluid. Whereas the observed mineral assemblages match predictions from the equilibrium phase diagram quite well, the actual reactions that

produced the final mineral assemblages appear to have been largely dictated by reaction kinetics, although possibly not very far from the equilibrium temperatures, with the possible exception of garnet.

The staurolite-consuming, andalusite- or sillimanite-forming reaction

In contrast, staurolite-bearing, chlorite-free rocks occur for a significant distance upgrade of the St + And isograd (Fig. 1b), even though staurolite is predicted to be completely consumed in the formation of andalusite only a short distance upgrade of the andalusite isograd (Fig. 12a). The patchy reaction of staurolite to andalusite in this broad interval suggests that: (i) staurolite is indeed metastable with respect to andalusite in this interval; (ii) the reaction of staurolite to andalusite was kinetically inhibited in many rocks; and (iii) local fluid presence lowered the kinetic barriers to nucleation and growth, allowing the reaction to proceed locally.

These features can be explained by the low $\Delta_r S_{P,T}$ of the staurolite-consuming, andalusite-producing reaction (4), resulting in small increase in reaction affinity with temperature overstep (Fig. 18). The low $\Delta_r S_{P,T}$ is due to the small amount of H_2O released per mole of andalusite produced (Table 3), contrasting with the higher vales of $\Delta_r S_{P,T}$ of the more substantially H_2O -producing, chlorite-consuming reactions. Figure 18a shows that the equilibrium temperature of reaction (7) has to be exceeded by 50–60 °C before the reaction affinity reaches 200 J mole^{-1} per oxygen in andalusite (equivalent to 1 kJ per mole of andalusite produced in the reaction).

The reason for the inhibited reaction of staurolite to andalusite may involve a combination of sluggish dissolution of staurolite, difficulty of nucleation of andalusite and slow nutrient transport in rocks lacking an intergranular fluid. Evidence in support of either or both of sluggish dissolution of staurolite and slow nutrient transport is the occurrence of euhedral staurolite crystals in rocks that contain andalusite (Fig. 3b), whereas evidence in support of nucleation difficulty of andalusite is the abrupt disappearance of staurolite once sillimanite is involved in the reaction. Although increasing temperature is also expected to result in accelerated reaction of staurolite, the abruptness of the change suggests kinetic control related to the involvement of sillimanite rather than andalusite in the reaction. Sillimanite is finer grained and more widely distributed throughout the matrix of the rock compared with discrete porphyroblasts of andalusite, indicative of easier nucleation. More widely distributed sillimanite would also favour growth because of smaller transport distances from reactant phase (staurolite) to product phase (sillimanite).

The importance of fluid in substantially reducing activation energy barriers to nucleation and growth of andalusite is apparent from the localized reaction of staurolite to andalusite in the wide zone between the andalusite and sillimanite isograds (Fig. 1b). This implies that the grain boundaries of most staurolite-bearing, chlorite-free rocks upgrade of the St + And isograd were volatile-deficient, indicating that the abundant H_2O generated earlier in the production of the staurolite from chlorite consumption escaped or was otherwise consumed. The source and driving mechanism for the localized influx of fluid that facilitated reaction of staurolite to andalusite is uncertain, but could be related to fluids released from the dehydrating intrusion, or channelled metamorphic dehydration fluids from below.

A final feature of this domain is the evidence for garnet growth in both the andalusite and sillimanite zones. The fact that garnet grew from a metastable staurolite-consuming reaction in a domain where it should instead have been consumed underscores the importance of kinetically controlled reactions in prograde metamorphism, especially in situations where the $\Delta_r S_{P,T}$ of the stable reactions is small. Table 3 shows that the $\Delta_r S_{P,T}$ of reaction (9), by which garnet is predicted to be consumed in the andalusite zone, is indeed extremely low.

Synthesis

Figure 18b provides a synthesis of the above interpretations in the form of a prograde path through reaction affinity–temperature space that qualitatively satisfies the range of spatial, textural and compositional features of the mineral assemblages in the aureole. The characteristic feature of the path in Fig. 18b is a sawtooth pattern that illustrates the interplay between equilibrium and kinetics in the progress of the reactions: intervals of reaction overstepping are marked by rises along the reactions, whereas intervals of reaction are marked by steep drops down towards equilibrium. The vertical drops to equilibrium shown in Fig. 18b imply that nucleation is the sole rate-limiting factor in reaction progress, whereas if porphyroblast dissolution and nutrient transport were also factors, as is likely the case, the drops would be less steep.

IMPLICATIONS FOR PROGRADE METAMORPHISM

Discrete intervals of reaction and of fluid generation in prograde metamorphism

Slowly increasing reaction affinity through broad multivariant domains in *P–T* phase diagram sections (pseudosections) may mean that reaction progress going through these domains is less than that predicted thermodynamically, and is unlikely to be continuous. Reaction may take place instead in abrupt, discrete intervals within these multivariant

domains, corresponding to the point at which sufficient reaction affinity has built up to overcome kinetic barriers to nucleation and growth. Reaction may not occur at all if the free energy change going through these domains is small, and metastable reaction is possible. These considerations contrast with the idea that most of the reaction that a metamorphic rock experiences along a *P–T*–time path occurs in broad multivariant domains, and call into question the notion of continuous equilibration during prograde metamorphism.

In the Nelson aureole, reaction was largely confined to three relatively narrow intervals corresponding to chlorite consumption, metastable reaction of staurolite to sillimanite, and muscovite consumption, with little or possibly no reaction between except where locally fluxed by fluids. Metamorphism was episodic rather than continuous, and fluid release (and possibly fluid presence in general) was correspondingly episodic rather than continuous (cf. Thompson, 1983; Rubie, 1986).

Nucleation difficulty and reaction overstepping

Several authors, such as Rubie (1998) and Waters & Lovegrove (2002), have argued that nucleation difficulty is an important, possibly leading, cause of reaction overstepping. Several aspects of this study support this inference, recognizing that the process of nucleation is linked to processes of reactant phase dissolution and intergranular transport needed to provide the nutrients to allow nuclei to initiate and grow. Overstepping of the garnet-in reaction is most plausibly explained by nucleation difficulty. Overstepping of the staurolite-out, andalusite/sillimanite-in reaction, the latter only proceeding significantly once sillimanite was involved, may be related to nucleation difficulty of andalusite compared with sillimanite, although sluggish dissolution of staurolite also appears to have played a role.

The estimated magnitude of nucleation-related overstepping of porphyroblast growth from a Ms + Chl protolith in this study (0–30 °C) is comparable with the lower end of the 30–40 °C estimate of Waters & Lovegrove (2002), but rather less than the 80 °C suggested by Zeh & Holness (2003) in their study of garnet growth from a Ms + Chl protolith in the Ilesha Schist belt of Nigeria. The success of the metamorphic facies principle, and the consistency of metapelitic mineral assemblage sequences in which the temperature difference between mineral assemblages is typically less than about 40 °C, argues against such extreme overstepping of devolatilization reactions of moderate to high $\Delta_r S_{P,T}$, other than in unusual circumstances. On the other hand, for reactions of low $\Delta_r S_{P,T}$ in dry rocks, more substantial overstepping is anticipated, as seen with the staurolite-out, andalusite/sillimanite-in reaction in this study.

Implications for thermobarometry and *P–T* path determinations

The results of this study indicate that the broad features of a metamorphic sequence may be accounted for by an equilibrium model, but that the details of isograd patterns, mineral textures, and mineral composition and chemical zoning require consideration of both equilibrium and kinetics. For example, a hitherto puzzling aspect of Area C of the Nelson aureole (Pattison & Vogl, 2005), which occurs immediately to the south of the study area, was the absence of an andalusite zone upgrade of staurolite development. Whereas this could be interpreted as an anomalously low thermal gradient adjacent to the igneous contact in this area, a more likely explanation is that, in the samples collected, no fluid infiltration had occurred to catalyse the reaction of staurolite to andalusite.

Although mineral assemblages may approach what is predicted from equilibrium thermodynamics, the results of this study suggest that the actual reactions leading to a given mineral assemblage may be quite different from those predicted by the phase equilibria. Some may be metastable, such as the staurolite-consuming, sillimanite-forming reaction. These considerations highlight the potential for misinterpretation of *P–T* paths when textures suggesting a particular sequence of mineral growth and consumption are interpreted solely with respect to the reactions in an equilibrium phase diagram, echoing points raised by Vernon & Powell (1976) and Vernon *et al.* (2008).

These results also introduce a note of caution to Powell & Holland's (2008) recommended approach to *P–T* estimation of metamorphic rocks, involving combined use of mineral assemblage stability domains in equilibrium phase diagram sections (pseudosections), measured mineral modes and compositions, and classical thermobarometry. The rationale for this approach is that all should agree, within uncertainty. In the Nelson aureole, by contrast, one predicts that they should not agree because some of the minerals (e.g. garnet and staurolite) occur outside their stability field and, in the case of garnet rims in the andalusite and sillimanite zones, grew metastably. Whether such a scenario could result in *P–T* discrepancies that fall outside the limits of uncertainty remains to be seen.

Application to regional metamorphism

Other studies of contact aureoles in which disequilibrium processes have been suggested include Hollister (1969a,b), Manning *et al.* (1993), Waters & Lovegrove (2002), Muller *et al.* (2004) and Buick *et al.* (2004). An important question is whether disequilibrium processes are restricted to contact metamorphic settings, or whether they extend to regional metamorphism. The timescales of regional metamorphism, and therefore heating rates, are generally considered to be slower than for contact metamorphism, although Waters &

Lovegrove (2002) argued that the timescale of metamorphism in the Bushveld aureole approached that of regional metamorphism.

Waters & Lovegrove (2002) noted that, according to classical, steady-state nucleation rate laws, the activation energy for nucleation depends inversely on the square of the temperature overstep, in contrast to other thermally activated processes (e.g. diffusion) whose activation energies are functions of absolute temperature but not of temperature overstep. The result is a sharp increase in nucleation rate over a very small temperature interval (a few degrees), and therefore a small dependence on heating rate. Ridley & Thompson (1986, p. 159) made the same point in arguing for the relevance of experimentally determined reaction oversteps to real metamorphic rocks. An exception could be the innermost zones of contact aureoles adjacent to hot intrusions, as argued by Buick *et al*. (2004).

A more significant factor may be the presence or absence of rock deformation occurring during metamorphism (Waters & Lovegrove, 2002). Deformation assists nucleation by building up strain energy in the reactant phases, contributing to the energy needed to overcome activation energy barriers, and by providing energetically favourable sites for nucleation. Deformation accompanying metamorphism is generally thought to be more common in regional metamorphism compared with contact metamorphism, although it is important to note that many contact aureoles show textures and structures indicative of deformation prior to and during metamorphism.

Evidence in support of lower degrees of overstepping in regional metamorphism compared to this study comes from the common occurrence of garnet zones of significant width downgrade of staurolite isograds in regional facies series 2b (staurolite-andalusite) sequences of the same pressure as this study (see examples in Pattison & Tracy, 1991). On the other hand, the fairly common occurrence of simultaneous 'staurolite + andalusite' and 'staurolite + kyanite' isograds in regional metamorphic settings, such as in Augusta, Maine (Osberg, 1968; Ferry, 1980) and Mica Creek, British Columbia (Ghent, 1975), respectively, and the common lack of evidence of instability of staurolite in kyanite-bearing rocks, may be suggestive of kinetically controlled processes similar to those that occurred in the Nelson aureole. Carlson (2002) demonstrated chemical disequilibrium during garnet growth from a number of regional metamorphic settings, further suggesting that disequilibrium during regional as well as contact metamorphism deserves consideration.

ACKNOWLEDGEMENTS

We thank J. Vogl (Univ. Florida) for his geological mapping and sampling of the Nelson batholith and aureole, which led to the identification of the study area. R. Marr (Univ. Calgary) is thanked for his assistance with the electron microprobe. M. Jolivet, S. Lallemand and their colleagues at Géosciences Montpellier are thanked for their hospitality during Pattison's half-sabbatical in 2006, when much of this work was done. D. Waters amiably clarified and debated several aspects of this study. D. Waters, W. Carlson, M. Brown and especially J. Ferry provided insightful reviews and editorial comments that improved the paper. This work was supported by NSERC grants 037233 to Pattison and 327218 to Tinkham.

REFERENCES

Andersen, T. B., 1984. Inclusion patterns in zoned garnets from Mageroy, north Norway. *Mineralogical Magazine*, **48,** 21–26.

Archibald, D. A., Glover, J. K., Price, R. A., Farrar, E. & Carmichael, D. M., 1983. Geochronology and tectonic implications of magnetism and metamorphism, Southern Kootenay Arc and neighbouring regions, southeastern British Columbia. Part I. Jurassic to Cretaceous. *Canadian Journal of Earth Sciences*, **20,** 1891–1913.

Buick, I. S., Stevens, G. & Gibson, R. L., 2004. The role of water retention in the anatexis of metapelites in the Bushveld Complex aureole, South Africa: an experimental study. *Journal of Petrology*, **45,** 1777–1797.

Burton, K. W., 1986. Garnet-quartz intergrowths in graphitic pelites: the role of the fluid phase. *Mineralogical Magazine*, **50,** 611–620.

Cairnes, C. E., 1934. Slocan Mining Camp, British Columbia. *Geological Survey of Canada Memoir*, **173**.

Carlson, W. D., 2002. Scales of disequilibrium and rates of equilibration during metamorphism. *American Mineralogist*, **87,** 185–204.

Chernoff, C. B. & Carlson, W. D., 1997. Disequilibrium for Ca during growth of pelitic garnet. *Journal of Metamorphic Geology*, **15,** 421–438.

Connolly, J. A. D. & Cesare, B., 1993. C-O-H-S fluid compositions and oxygen fugacity in graphitic metapelites. *Journal of Metamorphic Geology*, **11,** 379–388.

Cook, F. A., Green, A. G., Simony, P. S. *et al*., 1988. Lithoprobe seismic reflection structure of the southeastern Canadian Cordillera: initial results. *Tectonics*, **7,** 157–180.

De Capitani, C., 1994. Gleichgewichts-Phasendiagramme: Theorie und Software. *Ber. Deutsch. Mineral. Gesellsch.*, **72,** 48. (abstract).

De Capitani, C. & Brown, T. H., 1987. The computation of chemical equilibria in complex systems containing non-ideal solutions. *Geochimica et Cosmochimica Acta*, **51,** 2639–2652.

Ferry, J. M., 1980. A comparative study of geothermometers and geobarometers in pelitic schists from south-central Maine. *American Mineralogist*, **65,** 720–732.

Ghent, E. D., 1975. Temperature, pressure and mixed volatile equilibria attending metamorphism of staurolite-kyanite-bearing assemblages, Esplanade Range, British Columbia. *Geological Society of America Bulletin*, **86,** 1654–1660.

Ghosh, D. K., 1995. U-Pb geochronology of Jurassic to early Tertiary granitic intrusives from the Nelson-Castlegar area, southeastern British Columbia, Canada. *Canadian Journal of Earth Sciences*, **32,** 1668–1680.

Holdaway, M. J., 1971. Stability of andalusite and aluminum silicate phase diagram. *American Journal of Science*, **271,** 97–131.

Holland, T. J. B. & Powell, R., 1998. An internally consistent thermodynamic data set for phases of petrological interest. *Journal of Metamorphic Geology*, **16,** 309–344.

Holland, T. J. B. & Powell, R., 2003. Activity-composition relations for phases in petrological calculations: an asymmetric multicomponent formulation. *Contributions to Minerology and Petrology*, **145,** 492–501.
Hollister, L. S., 1969a. Contact metamorphism in the Kwoiek Area of B.C.: an end member of the metamorphic process. *Geological Society of America Bulletin*, **80,** 2465–2494.
Hollister, L. S., 1969b. Metastable paragenetic sequence of andalusite, kyanite, and sillimanite, Kwoiek Area, B.C. *American Journal of Science*, **267,** 352–370.
Jamtveit, B. & Andersen, T. B., 1992. Morphological instabilities during rapid growth of metamorphic garnets. *Physics and Chemistry of Minerals*, **19,** 176–184.
Kretz, R., 1983. Symbols for rock-forming minerals. *American Mineralogist*, **68,** 277–279.
Lasaga, A. C., 1986. Metamorphic reaction rate laws and development of isograds. *Mineralogical Magazine*, **50,** 359–373.
Little, H. W. 1960. Nelson map area, west half, British Columbia. *Geological Survey of Canada, Memoir*, **308**.
Manning, C. E., Ingebrisen, S. E. & Bird, D. K., 1993. Missing mineral zones in contact metamorphosed basalts. *American Journal of Science*, **293,** 894–938.
Meth, C. E. & Carlson, W. D., 2005. Diffusion-controlled synkinematic growth of garnet from a heterogeneous precursor at Passo Del Sole, Switzerland. *Canadian Mineralogist*, **43,** 157–182.
Muller, T., Baumgartner, L. P., Foster, C. T. & Vennemann, T. W., 2004. Metastable prograde mineral reactions in contact aureoles. *Geology*, **32,** 821–824.
Osberg, P. H., 1968. Stratigraphy, structural geology, and metamorphism of the Waterville-Vassalboro area, Maine. *Maine Geological Survey Bulletin*, **20**.
Parrish, R. R., 1992. U-Pb ages of Jurassic-Eocene plutonic rocks in the vicinity of the Valhalla Complex, southeastern British Columbia. In: *Radiogenic Age and Isotopic Studies: Report 5*. *Geological Survey of Canada Paper*, **91-2,** 115–134.
Pattison, D. R. M., 1992. Stability of andalusite and sillimanite and the Al_2SiO_5 triple point: constraints from the Ballachulish aureole, Scotland. *Journal of Geology*, **100,** 423–446.
Pattison, D. R. M., 2006. The fate of graphite in prograde metamorphism of pelites: an example from the Ballachulish aureole, Scotland. *Lithos*, **88,** 85–99.
Pattison, D. R. M. & Tracy, R. J., 1991. Phase equilibria and thermobarometry of metapelites. In: *Contact Metamorphism* (ed. Kerrick, D. M.), *Mineralogical Society of America Reviews in Mineralogy*, **26,** 105–206.
Pattison, D. R. M. & Vogl, J. J., 2005. Contrasting sequences of metapelitic mineral-assemblages in the aureole of the tilted Nelson Batholith, British Columbia: implications for phase equilibria and pressure determination in andalusite-sillimanite type settings. *Canadian Mineralogist*, **43,** 51–88.
Peacock, S. M., 1990. Numerical simulation of contact and regional metamorphism on the Macintosh microcomputer. *Journal of Geological Education*, **38,** 132–137.
Powell, R., 1998. Calculating phase diagrams involving solid solutions via non-linear equations, with examples using THERMOCALC. *Journal of Metamorphic Geology*, **16,** 577–588.
Powell, R. & Holland, T. J. B., 2008. On thermobarometry. *Journal of Metamorphic Geology*, **26,** 155–179.
Pyle, J. M. & Spear, F. S., 2003. Four generations of accessory-phase growth in low-pressure migmatites from SW New Hampshire. *American Mineralogist*, **88,** pp 338–351.
Rice, A. H. N. & Mitchell, J. I., 1991. Porphyroblast textural sector zoning and matrix displacement. *Mineralogical Magazine*, **55,** 379–396.
Ridley, J. & Thompson, A. B., 1986. The role of mineral kinetics in the development of metamorphic microtextures. In: *Fluid-Rock Interactions During Metamorphism* (eds Walther, J. V. & Wood, B. J.), pp. 154–193. *Advances in Physical Geochemistry, 5*, Springer-Verlag, New York.
Rubie, D. C., 1986. The catalysis of mineral reactions by water and restrictions on the presence of aqueous fluid during metamorphism. *Mineralogical Magazine*, **50,** 399–415.
Rubie, D. C., 1998. Disequilibrium during metamorphism: the role of nucleation kinetics. In: *What Drives Metamorphism and Metamorphic Reactions? Special Publication 138* (eds Treloar, P. J. & O'Brien, P. J.), pp. 199–214. Geological Society of London, London.
Sevigny, J. H. & Parrish, R. R., 1993. Age and origin of Late Jurassic and Paleocene granitoids, Nelson Batholith, southern British Columbia. *Canadian Journal of Earth Sciences*, **30,** 2305–2314.
Thompson, J. B., 1957. The graphical analysis of mineral assemblages in pelitic schists. *American Mineralogist*, **42,** 842–858.
Thompson, A. B., 1983. Fluid-absent metamorphism. *Journal of the Geological Society of London*, **140,** 533–547.
Tinkham, D. K. & Ghent, E. D., 2005. Estimating P-T conditions of garnet growth with isochemical phase diagram sections and the problem of effective bulk-composition. *Canadian Mineralogist*, **43,** 35–50.
Tomkins, H. S. & Pattison, D. R. M., 2007. Accessory phase petrogenesis in relation to major phase assemblages in pelites from the Nelson contact aureole, southern British Columbia. *Journal of Metamorphic Geology*, **25,** 401–421.
Vernon, R. H. & Powell, C. M., 1976. Porphyroblastesis and displacement – some new textural criteria from pelitic hornfels – reply. *Mineralogical Magazine*, **40,** 787–788.
Vernon, R. H., White, R. W. & Clarke, G. L., 2008. False metamorphic events inferred from misinterpretation of microstructural evidence and P-T data. *Journal of Metamorphic Geology*, **26,** 437–449.
Vogl, J. J. & Simony, P. S., 1992. The southern tail of the Nelson Batholith, southeast British Columbia: structure and emplacement. *Geological Survey of Canada Paper*, **92-1A,** 71–76.
Walther, J. V. & Wood, B. J., 1984. Rate and mechanism in prograde metamorphism. *Contributions to Mineralogy and Petrology*, **88,** 246–259.
Waters, D. J. & Lovegrove, D. P., 2002. Assessing the extent of disequilibrium and overstepping of prograde metamorphic reactions in metapelites from the Bushveld Complex aureole, South Africa. *Journal of Metamorphic Geology*, **20,** 135–149.
Wilbur, D. E. & Ague, J. J., 2006. Chemical disequilibrium during garnet growth: Monte Carlo simulations of natural crystal morphologies. *Geology*, **34,** 689–692.
Yardley, B. W. D., Condliffe, E., Lloyd, G. E. & Harris, D. H. M., 1996. Polyphase garnets from western Ireland; two-phase intergrowths in the grossular-almandine series. *European Journal of Mineralogy*, **8,** 383–392.
Zeh, A. & Holness, M. B., 2003. The effect of reaction overstep on garnet microtextures in metapelitic rocks of the Ilesha Schist Belt, SW Nigeria. *Journal of Petrology*, **44,** 967–994.

Received 17 October 2008; revision accepted 11 March 2009.